Waste and Biomass Valorization (2025) 16:3195–3214
https://doi.org/10.1007/s12649-024-02835-3

ORIGINAL PAPER

Quench-Layer-Based Model for Leaching Prediction of MSWI Bottom Ash

E. Loginova[1] · M. A. Proskurnin[2] · K. Schollbach[1] · H. J. H. Brouwers[1]

Received: 2 August 2023 / Accepted: 24 November 2024 / Published online: 28 December 2024

Abstract

Purpose The water-based cooldown process (quenching) of Municipal Solid Waste Incineration Bottom Ash (MSWI BA) after incineration may adversely affect its leaching by forming a highly contaminated quench layer on BA particles. A model is proposed to rapidly estimate the leaching of potentially toxic elements from this MSWI BA quench layer.

Methods The semi-empirical model is based on calculating the quench-layer-to-core ratio for size fractions for the particle size range from < 63 µm to > 22.4 mm and building leaching profiles for each element. A particle core and quench layer get assigned contribution values based on only two experimental points: leaching data for the largest (the minimum role of the quench layer) and smallest (quench layer domination) fractions of the test sample.

Results The calculated leaching profiles for major anions, alkali and alkaline-earth metals, and copper for a set of 18 narrow fractions demonstrate good leaching prediction, the underestimation error is –(10–20)%. For Ba, Sr, and Sb, the model provides a satisfactory error of 30% mainly due to contribution of core leaching; for Ni, Mn, and Zn, > 50%.

Conclusion Adequate modelling for most elements shows that, despite MSWI BA complexity, a simple semi-empirical model can predict the leaching behavior using a limited experimental dataset and supports the assumption of quench layer contribution to the total MSWI BA leaching.

Graphical Abstract

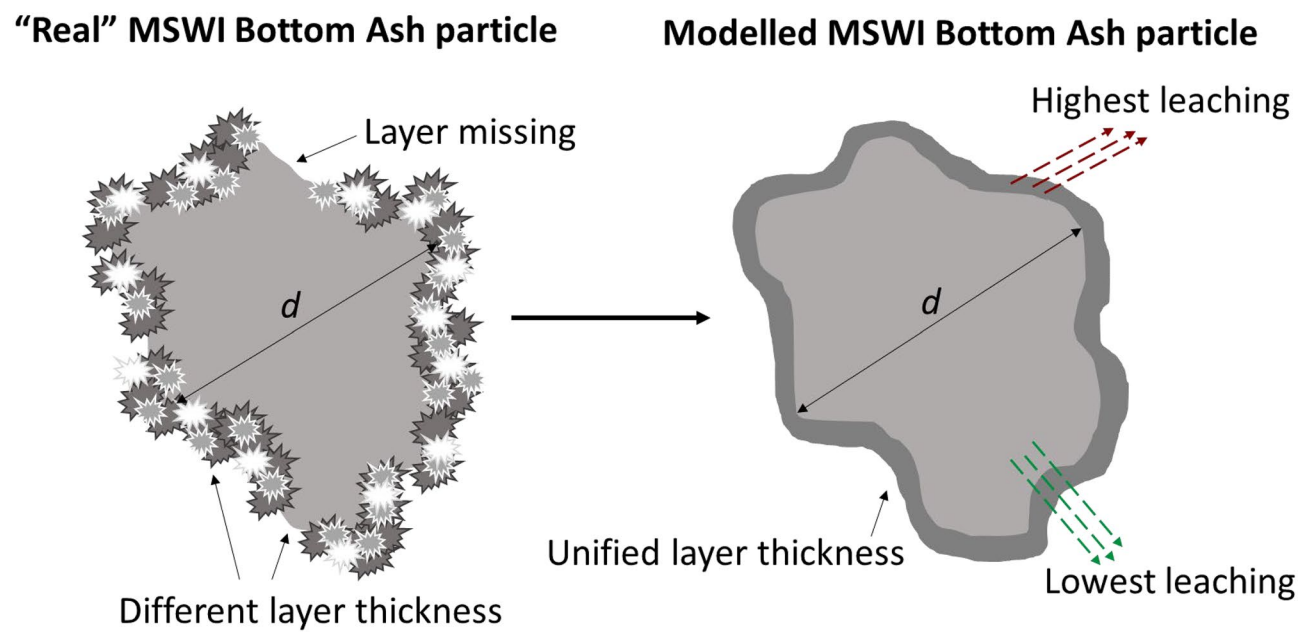

Keywords MSWI bottom ash · Leaching · Environmental impact · Quench layer · Leaching model

Extended author information available on the last page of the article

Introduction

Municipal Solid Waste Incineration Bottom Ash (MSWI BA) is one of the byproducts of the incineration process to reduce the volume and mass of household waste [1]. From circular-economy and environmental viewpoints, the recycling of MSWI BA is a relevant task. In the last decades, extensive research has dealt with various aspects of MSWI BA analysis and characterization [2–8], treatments [2–5, 9–11], and applications [1, 3–5, 9, 12, 13]. Specifically, numerous studies have focused on the leaching behavior of potentially toxic elements (PTEs), factors affecting it, and mitigating approaches [5, 12, 14–18]. In addition, quite a few studies have focused on the physical, chemical, mineralogical, and morphological properties of MSWI BA [4, 7, 19–25]. Over the years, many treatments have been suggested to minimize the adverse effects of this material if it is recycled as aggregates, road-base materials (coarse fractions) or cement replacement (fine fractions), such as thermal treatment, metal extraction to reduce the leaching, particle size separation, carbonation, etc. [10, 26–30].

It is challenging to reuse not only coarse fractions of MSWI BA but also fine fractions, which are more contaminated [4, 31] though have potential as a cement replacement [4, 22, 28–30, 32]. At the same time, PTE leaching remains one of the most acute challenges due to the high cost of treatments such as washing or sintering and sometimes limited effectiveness [33–35].

MSWI BA is highly inhomogeneous consisting of various types of matter, including rocks, glass, metal, unburned organic material, and incineration and weathering products [21, 36]. The composition of this incineration product is affected by the starting composition of the household waste, incineration conditions, and the cooling process [22, 31, 37, 38]. Most commonly, hot MSWI BA is cooled down by water quenching after incineration [31, 37]. Many changes occur to MSWI BA during this procedure due to dissolution, precipitation, and the reaction of salts and minerals and their reabsorption by newly forming structures [21]. The quenching process results in a somewhat unstable quench product layer containing or encapsulating PTEs and, has high to moderate concentrations of salts, particularly, chloride, sometimes from the quenching solution, and ash particles formed during incineration [31, 39, 40]. Thus, quenched MSWI BA particles above a size of ca. 250 µm typically contain a solid core covered with this quench product layer with fine particles interspersed with newly formed hydrates, mainly calcium silicate hydrates (CSH) [33, 40, 41]. BA particles below this size tend to consist primarily of this quench layer (as large particles barely participate in the formation of the quench products) [31, 37]. This means the finer the fraction, the more contaminated it is.

Several Ca-based minerals are formed only at the quenching stage, which can incorporate and immobilize PTEs. The literature mainly focuses on the behavior of chloride in this layer, as it tends to be the element leaching at the highest concentrations [6, 42]. The mineral crucial for chloride immobilization is Friedel's salt, $3CaO{\cdot}Al_2O_3{\cdot}CaCl_2{\cdot}10H_2O$, which only forms during quenching and cannot be removed easily (even by thermal treatment at 1000 ºC) [39]. It is considered the primary host of the insoluble chlorine in MSWI BA. Yang et al. also demonstrated that the quench products are the primary source of chlorine leaching in MSWI BA, resulting from the entrapment of tiny particles rich in Cl during the layer formation, found by SEM–EDX mapping analysis [39]. Inkaew et al. reproduced the quenching process under laboratory conditions to investigate its formation in-depth [31]. They showed that MSWI BA changes dramatically after quenching due to the formation of amorphous and microcrystalline CSH phases [23] and that the formation of the quench layer is governed by the presence of fine particles (< 425 µm). Due to their chemical composition, those particles aid the formation of the quench layer, and if separated from the coarser fraction before the quenching procedure, almost no layer is formed. They also found that the quench layer is approximately 0.01–1 mm thick (for particles of a size of 2 to 4 mm) [31]. Additionally, quenching water raised some concern as an apparent secondary origin of chloride in MSWI BA [42].

For the range of elements including PTEs, the literature body on the role the quench layer of MSWI BA in leaching and potential use of the quenched material is relatively scarce [4, 6, 31, 37]. Apart from the above-mentioned studies of quench-layer reproduction [31, 40], only limited information is available about other elements such as Cu, Zn, Ni, Cr, Sb, etc. [25, 43]. It was discovered that slow and soft milling performed on the MSWI BA fraction of 0.125–3 mm increasing the leaching of the material by removing fine contaminated particles from the quench layer and releasing the soluble salts attached to CSH [4]. This suggests that the quench layer might be responsible for leaching from MSWI BA to a great extent and should be studied further to understand its influence [4, 6, 37]. It might also be a key to estimating the leaching potential of MSWI BA and optimizing leaching-reducing treatments such as grinding or washing.

From a broader viewpoint of MSWI BA modelling, the existing models of MSWI, including MSWI BA, are numerous but mainly focused on the residue composition or environmental impact [9, 24, 44–46], especially on the impact related to the incineration process itself [47, 48]. Other studies are based on chemical-equilibria models [5, 12, 15] or geological models [9, 45, 46] and related to how the leaching of hazardous metals is affected by pH during long-term aging (weathering, carbonation, etc.) [49–51]. Also, numerical models of leaching are proposed, e.g. Park

and Batchelor made a multi-component numerical leaching model and showed its potential to improve or substitute for a standard leaching test [52]. Also, Dijkstra et al. used a pH-dependent computer model to predict the PTE leaching from MSWI BA with an accuracy of approximately an order of magnitude [15, 53]. Later, a multisurface geochemical model was developed to predict the simultaneous leaching of a range of elements from BA [54].

However, these models did not usually examine the quench layer but rather consider the whole composition of MSWI BA as a source of leaching. Moreover, usually building a model pursues a goal of demonstrating the adverse effects of the quench layer, which generally require in-depth knowledge about MSWI BA mineralogy that is complex and difficult to assess. They are therefore hard to use in practice to estimate leaching behavior of a generic BA batch. Thus, the approach to study the influence of the quench layer may be modeling based on experimental leaching data. In the previous study [25], certain similar S-shaped leaching patterns were obtained for multiple elements, yet the leaching data did not correlate with the specific surface area or the particle size. There was also no correlation found between the total content of the element in MSWI BA and its leachable amount. Because the acidity of the studied leachates varied only within pH 8.8–9.2, this parameter also could not justify the difference in the leaching among different particle-size fractions.

In this paper, a semi-empirical leaching model is proposed to demonstrate the viability of the hypothesis that the quench layer is seriously responsible for the leaching of certain elements [4] and can be used to estimate the leaching of MSWI BA for these elements and total leaching. The second aim was to demonstrate a potential link between the presence of the quench layer on MSWI BA particles and leaching and to evaluate the severity of the quenching problem and demonstrate that this way of handling MSWI BA prevents it from being easily transformed into a secondary material and requires several decontamination steps.

Materials and Methods

Samples and Instrumentation

The untreated (unwashed) but water-quenched (immersion of hot material into the quenching filtered tap water) and weathered MSWI BA was supplied by the municipal solid waste-to-energy incinerator plant of Mineralz (Duiven, the Netherlands), where they underwent the standard washing and ferrous and non-ferrous metal removal process. The material had been stored for 3 months after production, prior to the study. Two different batches (particle size range 0–22.4 mm, 15 kg each set) from the same furnace collected at the same time were used. The analyzed MSWI BA samples were initially pre-crushed at the plant to remove cemented matter and metals. Three replicate measurements were used for each leaching test.

Further, the material was oven-dried (105 °C; a UF 260 drying oven, Memmert GmbH, Germany) to a constant mass. Next, each set was sieved into 18 size fractions (sieve size: 63, 90, 125, 180, 250, 355, 500, and 710 µm, and 1.0, 1.4, 2.0, 2.8, 4.0, 5.6, 8.0, 11.2, and 22.4 mm) according to EN 933–1 (2012) and EN 933–2 (1995); all the sizes were representative to make microelement and anion analysis. Median particle size and specific densities for each sieve fraction as well as the pH of the leachate after the standard leaching test (BS EN 12457–4:2002) are summarized in Table 1. All the particles of a size fraction are given an average size, which is the arithmetic mean, median, of the minimum and maximum sizes of this fraction (e.g., a fraction named «180 µm» shows the largest size and has a range from 125 to 180 µm, and therefore the median, is 152.5 µm, Table 1). This median value was used as the particle characteristic size for the model to build numerical plots.

Each fraction of both sets was divided with sample splitters (15-D0438 riffle boxes, CONTROLs Group) into 4 parts, 3 of which were used for the standard leaching test by BS EN 12457–4:2002, 24 h shaking, L/S 10, 200 rpm on an SM-30 shaking table (Edmund Bühler GmbH). After the test, the leachates were filtered through 0.2-µm filters to prepare solutions for ion chromatography and inductively coupled plasma optical emission spectroscopy (ICP–OES,

Table 1 Parameters of the used MSWI BA sieved fractions

	Sieve size	Median particle size	Specific density (g/cm^3)	pH
µm	63	31	2.6	8.9
	90	77	2.6	8.9
	125	108	2.7	8.8
	180	153	2.7	8.8
	250	215	2.7	8.8
	355	302	2.7	8.8
	500	427	2.7	8.8
	710	605	2.7	8.9
	1000	855	2.8	8.9
mm	1.4	1.2	2.9	9.1
	2.0	1.7	2.8	9.1
	2.8	2.4	2.9	9
	4.0	3.4	2.8	9.2
	5.6	4.8	2.8	9.1
	8.0	6.8	2.7	9.1
	11.2	9.6	2.7	9.1
	22.4	16.8	2.8	9.1
	31	22.4	2.9	9.2

for the latter, filtrates were stabilized with nitric acid). A chamber furnace (Thermo Scientific Heraeus K 114) was used for loss on ignition (LOI) at 550 °C [25].

Further microelement analyses (Na, K, Mg, Ca, Sr, Ba, Cu, Mn, Ni, Zn, Sb, Cr, Pb, Sn, Ti, V, Si, and S) were performed by an ICP–OES 5100 SVDV spectrometer (Agilent Technologies, USA). Chloride and sulfate were determined by ion chromatography, a Thermo Scientific Dionex 1100 ion chromatograph. Specific densities of dried samples were measured by a Helium AccuPyc II 1340 pycnometer. Other details of ICP–OES and ion-chromatographic analysis are given in [25].

Model Concept and Assumptions

The leaching of the finest fraction (< 63 µm) was taken as responsible for the leaching of the quench layer, because it can be assumed to consist mostly of broken-off quench product [4, 31]. The largest fraction is the least affected by the presence of quench products [4]; therefore, its leaching value was used as the background leaching of the core material. Two parameters are needed to calculate the modelled total leaching value (L_{total}): ratios of $R_q = V_q/V_p$ and $R_c = V_c/V_p$ for each fraction, where V_q, V_c, and V_p are volumes of the quench layer, core, and the whole particle, respectively. As the core and the whole particle are assumed to have similar round shape, $R_c = \sqrt[3]{(r-K)/r}$ and, thus, $R_q = 1 - \sqrt[3]{(r-K)/r}$. Here, r is half the particle characteristic size d and K is the quench layer thickness. More details on calculations are given in the Supplementary Information.

The value of K, the unified layer thickness (Fig. 1), is selected by fitting the layer thickness to the empirically obtained leaching values from the previous findings [31] and the analysis of the quench layer and is removal by washing and grinding of the same MSWI BA product [4, 22, 25]. The result is 20 µm, which gives the best fit for all elements, and which is subsequently used for the second, validation data set. The values for the quench layer thickness suggested by the literature are 10–1000 µm [31], with the most characteristic values for fine-to-medium particle sizes of 10–50 µm [4, 31], which agrees well with the layer selection of the present model by the leaching values.

Further, each R_q was normalized to the R_q value of the finest fraction (R'_q), and the same was done to R_c but to the core value of the largest fraction (R'_c). This way, the range of values was obtained for each fraction indicating how the percentage of the quench layer compared to the core changes depending on the particle size. Because the ratio between the leaching volume and the core decreases with increasing particle size, the leaching of the largest fraction is lowest. The model applies the ratios of the quench part (leaching of the most contaminated, fine fraction) and the core (leaching of the least contaminated, coarse fraction) to the total volume of the particle for each fraction.

Leaching Estimation

The model predicts the leaching value for a certain element of a target fraction as:

$$L_X = R'_q L_f + R'_c L_l \quad (1)$$

Here, L_X is the leaching value for the target fraction X; L_f and L_l are experimental leaching values for the finest and

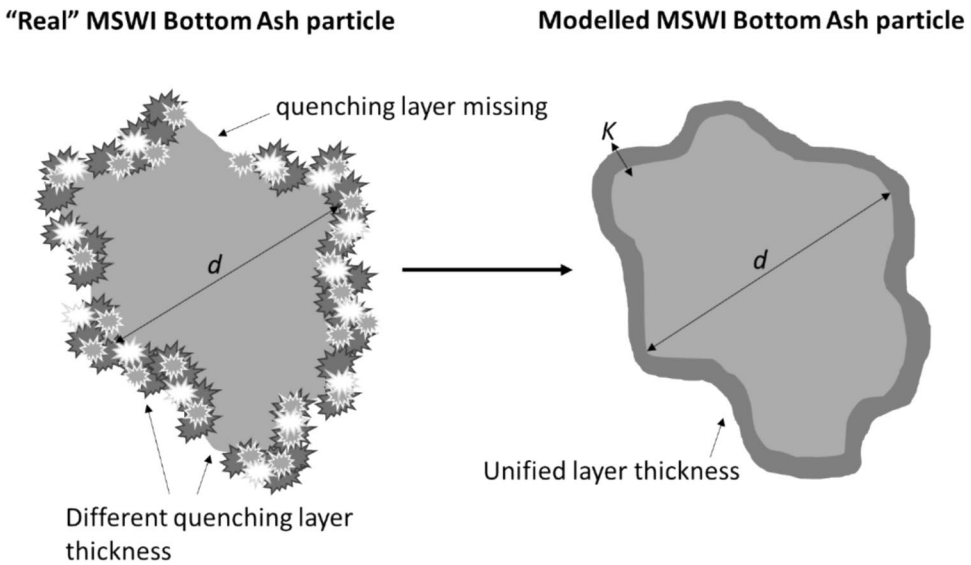

Fig. 1 Schematic representation of a BA particle, "real" (left), modelled (right); d is average particle size; K represents an averaged, equal thickness of the quench layer for all MSWI BA particles throughout the fractions

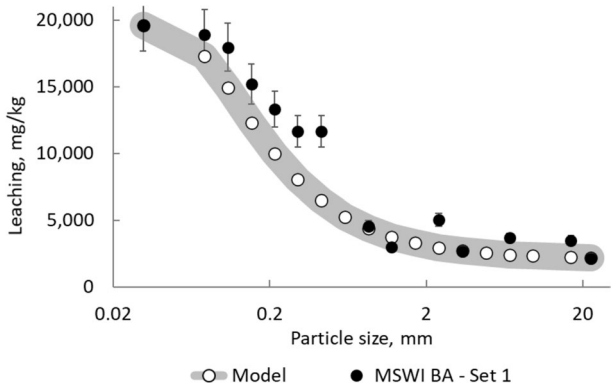

Fig. 2 Example of the modeled and measured leaching values (chloride). The error bars are standard deviations for each measurement done in triplicate

largest fractions, respectively. The density of the core and the quench layers might differ slightly, yet the data on the specific density indicates that the difference is insignificant, therefore the same density for the core and the quench layer is used in this model.

For each element, L_X, Eq. (1), was calculated for each of 16 fractions other than the finest and the largest to obtain the range of modelled leaching values, altogether for a single element they were portrayed as a curve and compared to the values from the experimental sets (Fig. 2 as an example).

To assess the model accuracy for each element, the sum of the relative standard deviations (RSD) was calculated for the data points (pairs) for all particle size fractions, obtained in the experiment and modeled (Table 2).

Results

The concept of the proposed model is to incorporate the relative leaching data (mg/kg) from the entire particle size-fraction range to estimate the influence of the quench layer in PTE leaching. The model assumes that all particles, regardless of their size, have a quench layer of equal thickness, which is supported with the previous findings [4, 31]. The model is based on the idea that leaching occurs primarily from this quench layer, but the potential contribution to leaching from the core is also considered. Figure 1 shows the abstraction made from real particles of MSWI BA with non-uniform to the model with a unified, median quench-product layer thickness, the main assumptions made in the model are given in Supplementary Information (Figure S1).

The main objective of this study was to demonstrate the effect of the quench layer on the short-term leaching (24 h shaking) through the entire range of fractions. Two sets of the leaching data for different representative particle size fractions, which are previously characterized by the total composition, morphology, and leaching and are representative for this MSWI BA [4, 22, 25] are obtained, see the Supplementary Information, Tables S1 and S2. The additional sieves with the mesh sizes of 22.4 mm, 11.2 mm, 5.6 mm, 2.8 mm, 1.4 mm, 710 µm, 355 µm, 180 µm, and 90 µm were

Table 2 Coefficients of correlation and precision of the proposed leaching model for test elements

Element	Building set			Validation set		
	R	RSD sum for all fractions	Total estimation error, %	*R*	RSD sum for all fractions	Total estimation error, %
Sulfate	0.98	1.23	− 8.3%	0.95	1.88	− 13.8%
Chloride	0.97	0.90	− 15.3%	0.97	1.35	− 10.5%
Sodium	0.98	0.93	− 13.3%	0.98	0.90	− 11.2%
Potassium	0.98	1.07	− 15.1%	0.97	0.97	− 12.7%
Magnesium	0.96	1.16	− 17.0%	0.95	1.30	− 16.8%
Calcium	0.94	1.88	− 17%	0.93	2.22	− 16.3%
Strontium	0.96	1.90	− 10.4%	0.89	2.50	− 11.5%
Copper	0.96	2.07	− 16.8%	0.97	2.40	− 23%
Zinc	0.89	33.6	+ 54.6%	0.86	74.2	+ 73.9%
Manganese	0.82	4.8	− 35.6%	0.81	6.6	− 37.1%
Barium	0.73	2.46	+ 29.7%	0.56	3.65	+ 33.2%
Antimony	0.80	0.28	− 1.8%	0.65	0.39	+ 1.9%
Nickel	0.39	9.68	− 71.4%	0.58	9.0	− 66.2%

added to the standard sieve set of EN 933–1 (2012) and EN 933–2 (1995) to obtain a larger number of narrower fractions and, thus, a better specification within the whole MSWI BA sample. One set was used to create the model, and the other, to validate it. A more detailed discussion of the whole composition and leaching in the entire particle size range of samples of this source of MSWI BA was published previously [25]. The elements with leaching concentrations below LOQs by ICP–OES (or < 0.05 mg/kg recalculated to the sample mass) for the majority of the fractions (Co, Cr, Mo, Pb, Sn, Cd, and V) were excluded as either not suitable for model or providing high instrumental errors. Ti was not considered as accumulated mainly in fly ash [11, 13] and also showing rather negligible leaching. Leaching of Fe and Al were also disregarded, as they do not leach significantly from MSWI BA [25]. Thus, the leaching behavior of chloride and sulfate, Na, K, Mg, Ca, Sr, Ba, Cu, Mn, Ni, Zn, and Sb, as well as total S and total Si, was considered as typical elements present in MSWI BA. The procedure of model building and validation was made using Set 1 to create the model and Set 2 to validate it and vice versa; the parameters of the model curves and coefficients of correlation differ insignificantly.

Experimental and Calculated Leaching Curves

The calculation, Eq. (1), was made for the entire set of selected elements for 18 size fractions. Figure 1 illustrates the graphical model representation including calculated data points for chloride. Figures 3, 4, 5, 6, 7, 8 and Fig. S3 (the Supplementary information) present the leaching results from data Sets 1 (as building) and 2 (as validating) and the modelling results. The leaching curve shape of most of the selected elements and for total leaching agrees well with the existing data [8, 25, 55]. The model shows a good fit for chloride, sulfate, Na^+, K^+, Ca^{2+}, Mg^{2+}, and Sr^{2+} (Figs. 3–5), overestimated values for Ba^{2+}, Zn^{2+} and Sb^{2+} and underestimated values for Cu^{2+} (Figs. 6 and 7), and no good fit for Mn^{2+} and Ni^{2+} (Fig. 8).

Table 2 presents the coefficients of correlation of model curves, the model precision as sums of relative standard deviations for each curve (element/ion), and overall, the

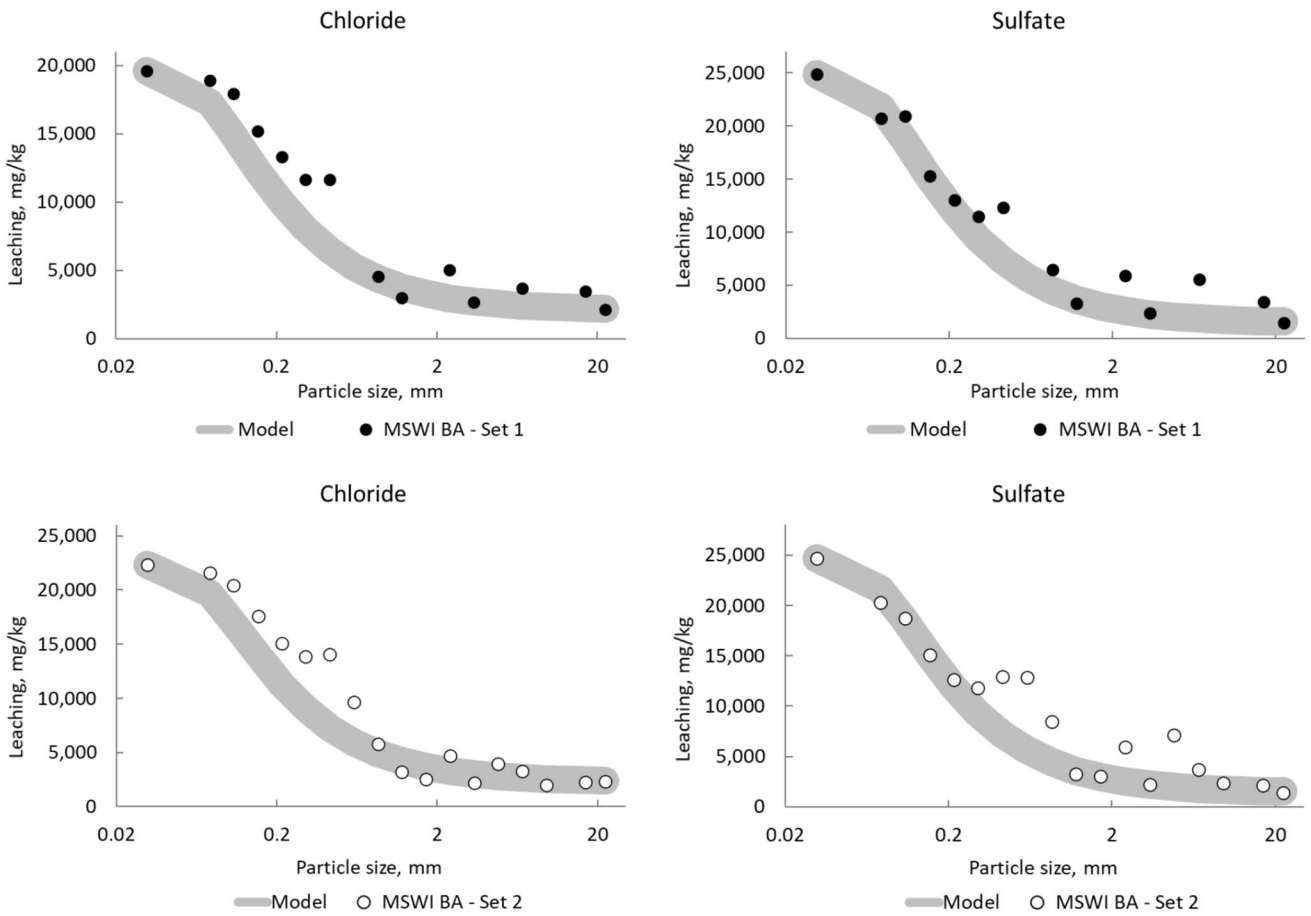

Fig. 3 Model behavior for chloride and sulfate; Set 1 is the experimental and Set 2 is the validation sets. Data points are the measured leaching values; gray curves are leaching values calculated based on the model

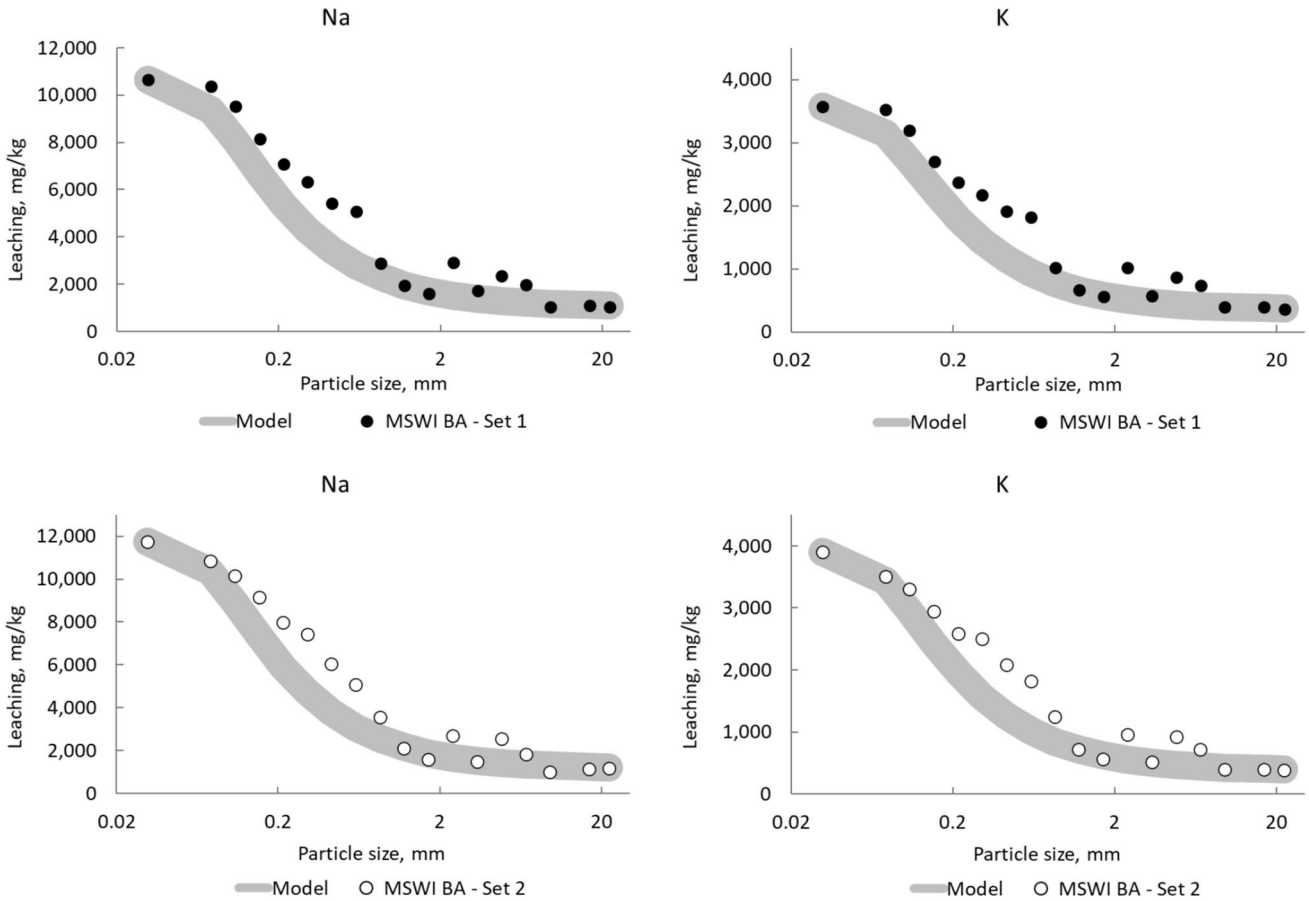

Fig. 4 Model behavior for Na and K; Set 1 is the experimental and Set 2 is the validation sets. Data points are the measured leaching values; gray curves are leaching values calculated based on the model

leaching errors, to objectively assess the quality provided by the model describing the leaching behavior of a particular element. It was calculated by obtaining the RSD for all the data points of two curves (Sets 1 and 2), and then summing them up for one element. The dependences of the errors for modelled values on the particle size are given in the Supplementary Information, Tables S1 and S2. The density did not vary significantly throughout the particle size range of the studied MSWI BA, but generally it cannot be assumed that unprocessed MSWI BA fractions would always have the same density due to differences in the treatment during and after the incineration. In fact, lower temperatures and incineration time might leave a higher degree of unburnt organic matter, or metal extraction can be more or less effective at different plants, therefore, it might be considered as an additional step to include the density correction in the calculations.

The leaching of silicate is minor (ca. 0.02–0.03% of total Si [25]) and almost does not depend on the particle size, Fig. S4 of the Supplementary information; only a small increase is observed for particle sizes above 2 mm due to the roughening in the particle shape. This could be considered a certain proof that Si leaching goes from the particle core, which is confirmed by the interelement correlations of silicon with almost all the elements, which are close to zero, Table S3, the Supplementary information. The percentage of leaching compared to total contents for all the selected elements for three coarsest fractions show the same independence from the particle size and confirms the previous findings of its leaching as CSH [33, 40, 41] and indifference for untreated and washed particles [25], which is reflected in the behavior of the leaching curves in this study (Figs 3, 4, 5, 6, 7, 8), which can be considered the leaching from the particle cores.

Total leaching curves, the sum of leaching for all the studied components (Fig. 9) show the least deviation from the model as it is dominated by the maximum leaching contributions from the least deviated elements of the group of well-fit components (Na, K, Mg, Ca, Sr, S, and Cu; sulfate and chloride). The coefficients of model correlation for total leaching are 0.98–0.99. The model generally shows some small underestimation of the total leaching of the entire range by

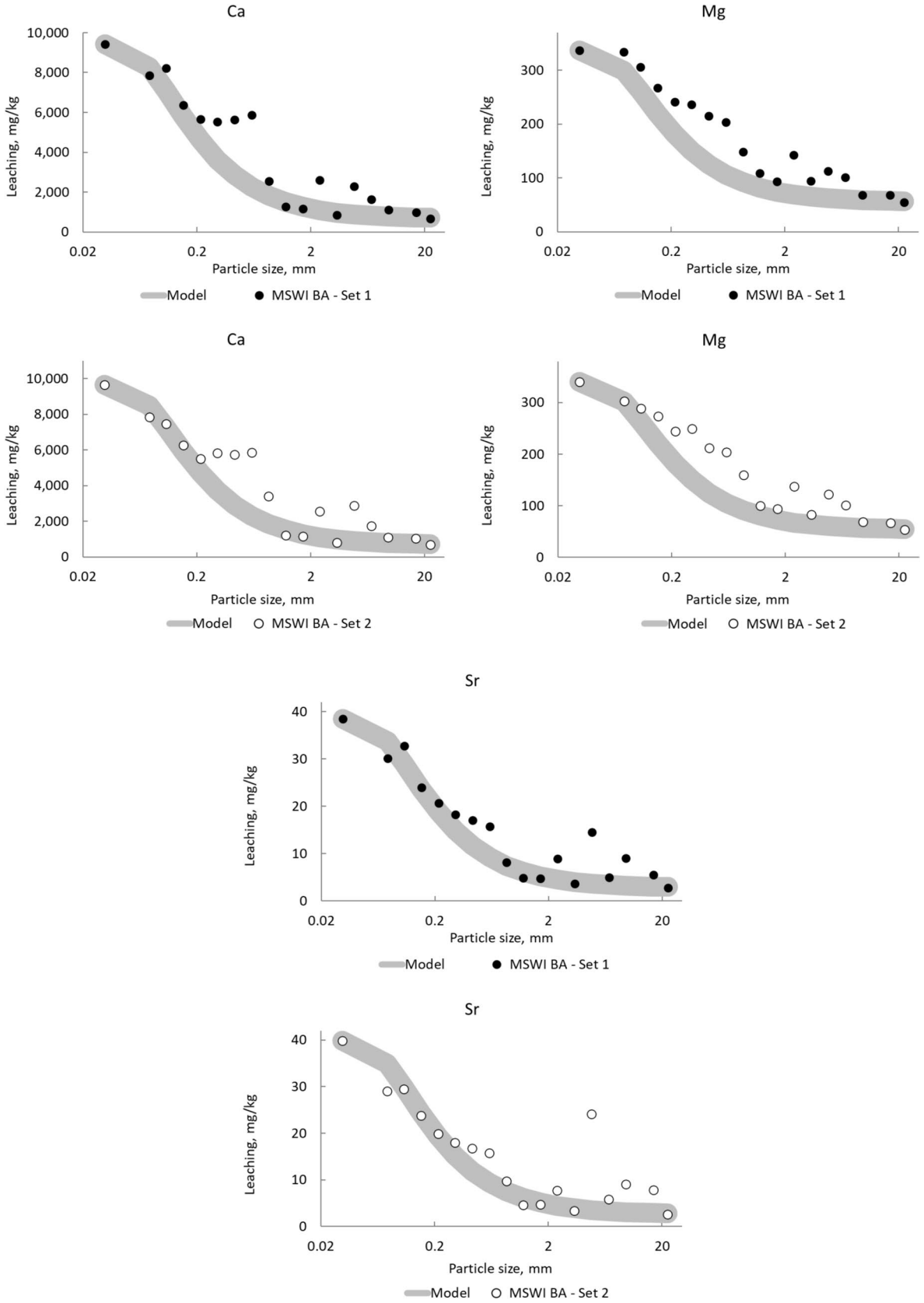

Fig. 5 Model behavior for Ca, Mg, and Sr; Set 1 is the experimental and Set 2 is the validation sets. Data points are the measured leaching values; gray curves are leaching values calculated based on the model

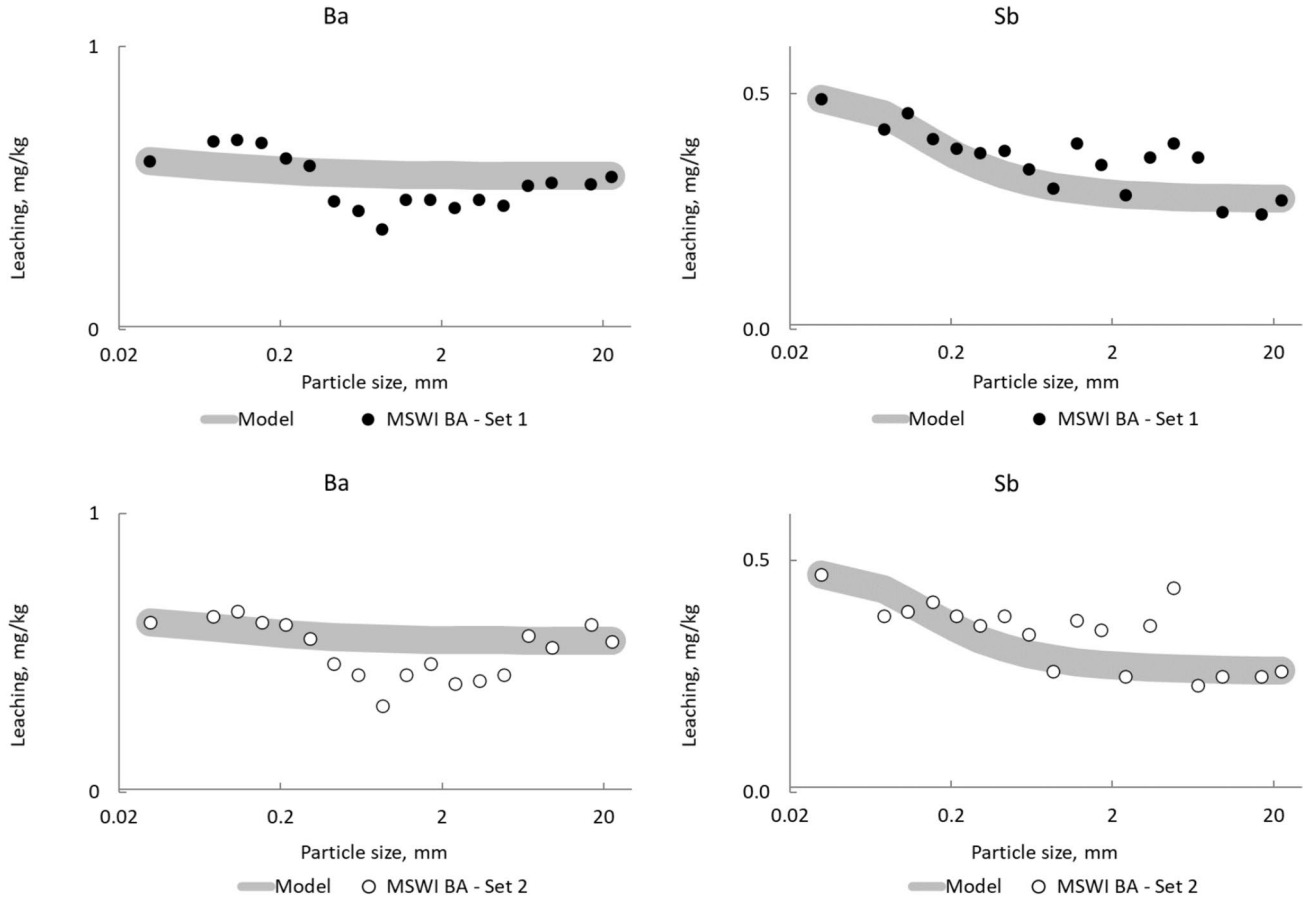

Fig. 6 Model behavior for Ba and Sb; Set 1 is the experimental and Set 2 is the validation sets. Data points are the measured leaching values; gray curves are leaching values calculated based on the model

5–7%, which results from higher leaching of phases of sizes of ca. 0.5 mm and 5 mm. Total leaching shown very high correlations with leaching of all the elements of the well-fit components.

Chloride and Sulfate

The coefficients of model correlation for both anions are in the range of 0.95–0.98 (Table 2). The RSD sum for the Set 1 is 0.9 and for the Set 2 is 1.35 (Table 2), thus underestimating the total leaching of the entire range by ca. 10–15%. For sulfate, the RSD sum for Set 1 is 1.23 and for Set 2 is 1.88, thus underestimating the leaching of the entire range by about 8–14%. As a whole, the model provides very good estimation of anion leaching for the total batch and for each fraction. The curve of sulfate (Fig. 3) is fully coincident with the curve for total sulfur for ICP–OES, Fig. S3 and Table S3 (the Supplementary information).

For both chloride and sulfate (Fig. 3) and total sulfur (Fig. S3), most fractions are estimated by the model fairly accurately (RSD < 0.1 for most of the fractions). The maximum underestimation, though slight, is in the range of 0.3–0.5 mm (RSD of 0.17). Similar results were observed for the experimental and validation sets (Supplementary Information, Figure S2). For Set 2, the least accurately described fraction is 1.4–2.0 mm with an RSD of 0.34. For sulfate and sulfur, the most deviating fractions are 4–10 mm with the RSD of 0.4–0.5.

Both anions show very high interelement correlations with all the elements of the first group (Na, K, Mg, Ca, Sr, S, and Cu), Table S3, the Supplementary information, with fairly high coefficients of correlations of other elements, which could be a proof that leaching goes from the quench layer filled with chloride and sulfate salts [6, 39, 42]. A very good correlation with the total-leaching curve (Fig. 9) is observed, the coefficients are over 0.99.

Sodium and Potassium

Figure 4 presents the data on alkali metals, for which the shape of the leaching curves throughout the fraction range was similar and correlated to anions. The coefficients of model correlation for both sets for sodium and potassium are 0.97–0.98 (Table 2). For sodium, the RSD sum is 0.9–1.0,

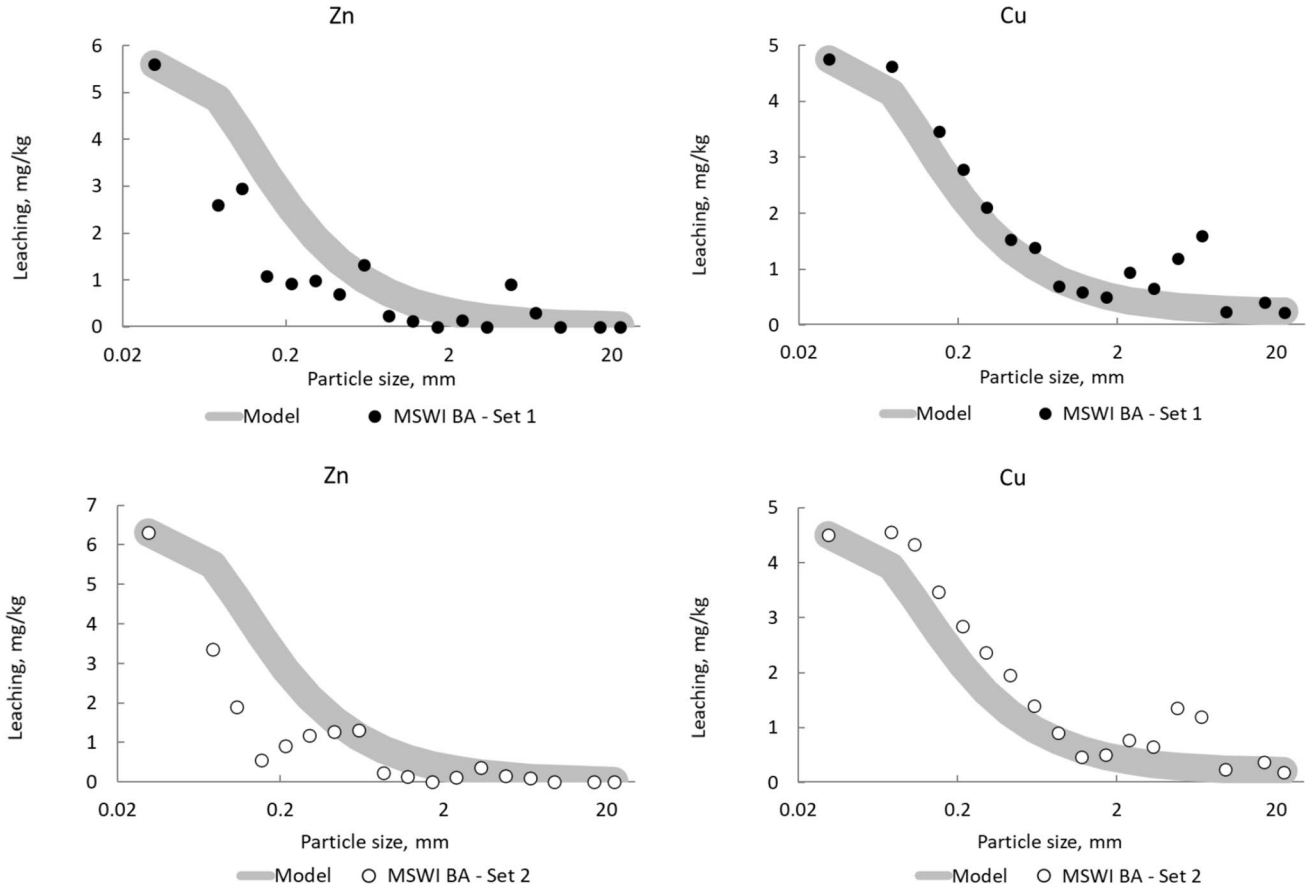

Fig. 7 Model behavior for Zn and Cu; Set 1 is the experimental and Set 2 is the validation sets. Data points are the measured leaching values; gray curves are leaching values calculated based on the model

thus underestimating the entire leaching range by about 11–13% for the whole sets; for potassium, RSDs are the same (Table 2), and the underestimation is 13–15%.

As for anions, sodium and potassium leaching concentrations are estimated fairly accurately for nearly all the fractions by the model (RSD < 0.1 for most of the fraction sizes); the most deviating fractions are 2.0–2.8 and 4.0–5.6 mm for sodium and 4.0–5.6 mm and 5.6–8.0 mm for potassium, RSDs are ca. 0.20. For the validation set, the same behavior was observed, the same RSD of 0.2. As for anions, the same slight underestimation is observed for the particle size range of 0.3–0.7 mm for N and K, which is slightly higher compared to anions. These results agree well with the literature because sodium and potassium are mainly present in salts with high solubility [42]. Therefore, the more soluble the compounds for a particular element are, the better the model is going to describe their behavior.

The interelement correlations of Na nd K are expectedly the same as for the anions, Table S3, the Supplementary information, with the same fairly high coefficients of correlations of other elements that show higher deviations of the model. A very good correlation with the total-leaching curve (Fig. 9) is observed; the coefficients are over 0.99.

Magnesium, Calcium, and Strontium

The coefficients of model correlation for the building set are over 0.95 for magnesium, over 0.93 for calcium, and over 0.96 for strontium, which is only a bit lower than for two main cations and anions (Table 2). The RSD sums for the building set are 1.2–1.3 and 1.9–2.2 for Ca and Mg, respectively, giving the error of –17% for both cations for both sets. For Sr, this underestimation of the entire-range leaching for ca. 10%, which is even better than for potassium and sodium.

For Mg and Ca, as for all cases described above, most of the fractions are estimated fairly accurately by the model (RSD < 0.1 for most of the data points). For Mg, the most deviating fractions are 2.0–2.8 mm and 4.0–5.6 mm (RSD, 0.23). Compared with K and Na, the maximum error range and the maximum error is the same. For Ca, the most deviating fractions are 0.71–1.0 mm and 4.0–5.6 mm with the RSD of 0.30–0.45. Comparing with K and Na, the maximum error

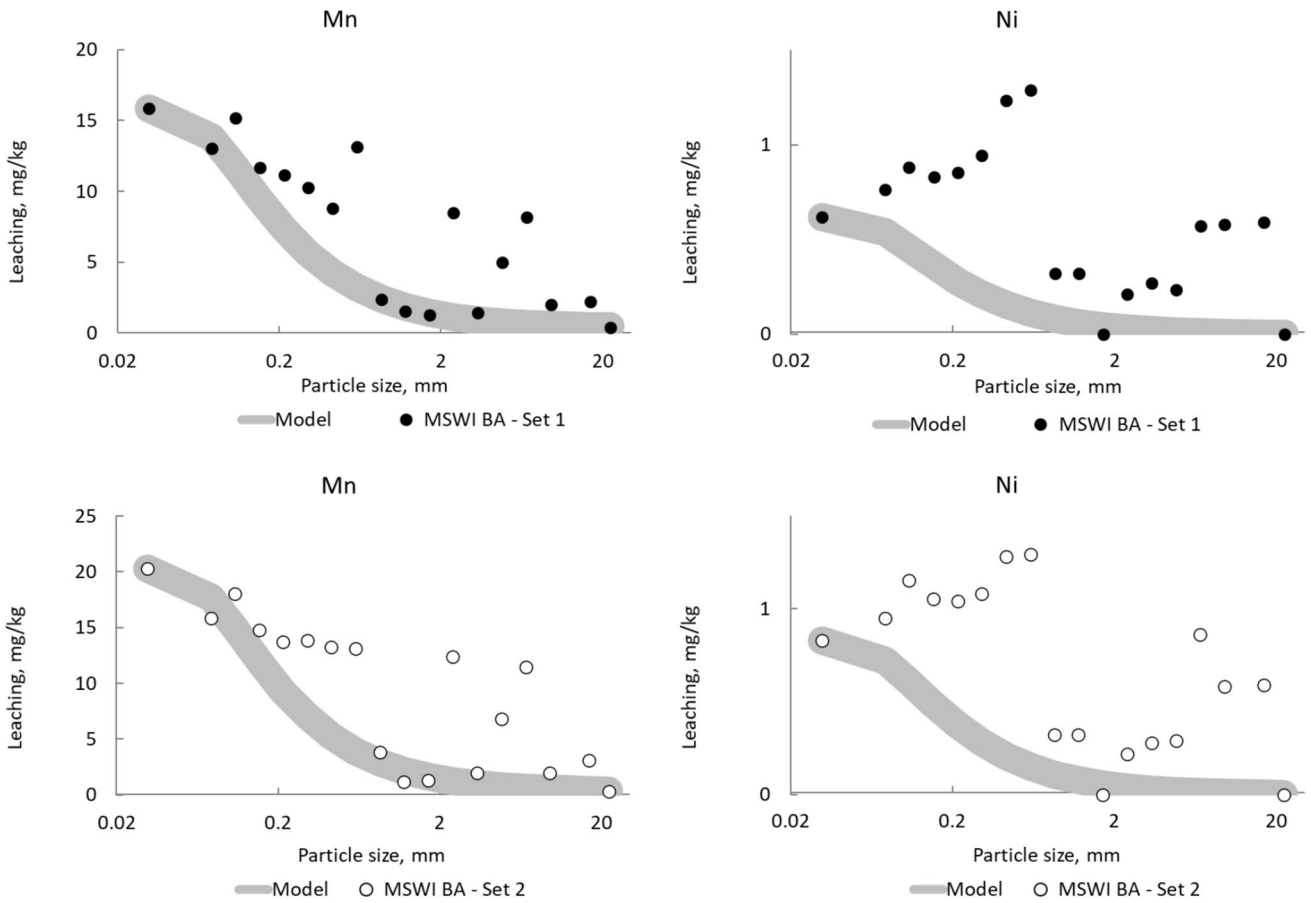

Fig. 8 Model behavior for Mn and Ni; Set 1 is the experimental and Set 2 is the validation sets. Data points are the measured leaching values; gray curves are leaching values calculated based on the model

range is the same but for Ca, the underestimation is higher. For Sr, the fine-fraction range, up to 1 mm, is described well by the model (RSD < 0.1 for most of the data points), but larger fractions show a high deviation. Three fractions out of 18 have the RSD in the range of 0.15–0.20, and the two most deviating fractions are 4.0–5.6 and 8.0–11.2 mm, with the RSD of 0.40 and 0.54, respectively.

Mg, Ca, and Sr show very high interelement correlations between each other and with Na, K, chloride, sulfate, and total S, Table S3, the Supplementary information, fairly high coefficients of correlations with Sb. However, the interelement correlations with Ba are rather low, and Ni shows coefficients of correlation with Mg, Ca, and Sr. Very good correlation with the total-leaching curve (Fig. 9) is observed; the coefficients are over 0.98.

Barium

The behavior of barium is quite different from Mg, Ca, and Sr. The coefficient of model correlation for Ba is the lowest among all the alkaline-earth elements, 0.73 and 0.56 for the building and validation sets. This results in overestimating the entire range of leaching values by about 30–33%, which is contrary to the overall underestimation for the rest of alkaline-earth elements and magnesium.

For individual fractions, the large-fraction range, from 1.4 mm is described well by the model (RSD < 0.1 for most of the data points), but the fine-fraction range is not described so accurately (Fig. S2, the Supplementary information). The two most deviating fractions are 500–710 µm and 0.71–1.0 mm with RSDs of 0.32 and 0.59, respectively.

The interelement correlations are different from all the above elements (Table S3, the Supplementary information), the coefficients of correlation are lower, and, as an exception, the interelement correlation with Si leaching significantly above zero, 0.4. This may mean that Ba leaching is not form the quench layer mainly, and represents the core leaching, which is confirmed by a much lower difference of the leaching value for the fine and the largest fractions (Fig. 6). It is worth noting that the coefficients of interelement correlation of Ba with sulfate/total S for large fractions are close to –1 that means that barium is expectedly leached from the core

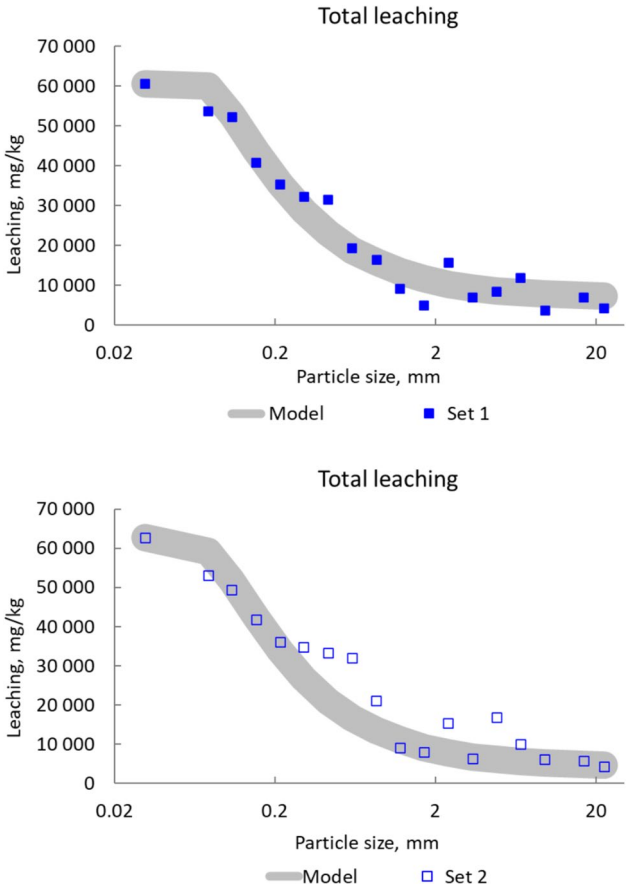

Fig. 9 Model behavior for total leaching; Set 1 is the experimental and Set 2 is the validation sets. Data points are the measured leaching values; gray curves are leaching values calculated based on the model

not as sulfate. To the contrary, the coefficient of interelement correlations of Ba and S for fine fractions is close to 0.7, which probably means that Ba leaches as particulate matter, fine particles of difficultly soluble compounds, which may then dissolve in presence of chlorides [56].

Copper

The coefficients of correlation for Cu are over 0.96, with the shape similar to Na, K, Mg, and Sr (Fig. 7). Also, as for the above elements of the first group (Na, K, Mg, Ca, Sr, and S; sulfate and chloride), the total RSD sum shows leaching underestimation for the entire range for ca. 17%. The fine-fraction range up to 2 mm is described well by the model (RSD < 0.1 for most points). The two most deviating fractions for both sets are the same, 4.0–5.6 and 5.6–8.0 mm, RSD of 0.5–0.6 (Figure S2, the Supplementary information), which partially coincides with other elements of the group. However, increased amounts of copper leaching in this range may indicate a change in copper species, especially less soluble oxides and silicates, as was previously shown by XANES analysis for several BA samples [57].

Interelement correlations of Cu are very close to 1 for all the elements of the first group (Table S3, the Supplementary information), and there is no correlation with Si leaching. Along with low leaching values for coarse fractions, this may be the evidence of copper leaching from the quench layer mainly.

Zinc

The coefficients of model correlation for Zn are above 0.86 (Table 2), which can be considered rather high; however, the RSD sums are significantly more than for above-described elements; for the Set 1, it is 33.6, and for the validation Set 2, 74.2. Contrary to other elements except Ba, the model results in the overestimation of the entire-range leaching by about 55–74% as nearly all fractions deviate significantly from the model. For the Set 1, only two points have the RSD < 0.15, and for the Set 2, five (Figure S2, Supplementary Information). The two most deviating fractions are 1.0–1.4 mm and 0.71–1.0 mm with the RSD of 14 and 5.9, respectively. One of the many reasons for that could be the difference of this fraction (based on visual inspection) in comparison with the fine fractions (looking like dark gray sand), and the coarse fractions (particles of rocks, glass, ceramics, etc.). Therefore, this fraction might be an outlier. Furthermore, very little Zn leaching is observed throughout all fractions, and for the particle size range from 1 to 22 mm, the values are fairly similar and close to zero (Fig. 7), unlike the descending trend among large fractions, which can be observed for elements with a good fit [58]. The metal extraction treatment after the incineration might play a role in it.

Interelement correlations of Zn with other elements (Table S3, the Supplementary information) show no correlation with Si leaching and rather fair correlations with all other elements (ca. 0.6–0.7).

Antimony

For antimony (Fig. 6), the coefficient of correlation for the Set 1 is 0.8, and for the Set 2 is 0.65. The RSD sum for the Set 1 is 0.28, and for the Set 2 is 0.39. This results in underestimating the entire-range leaching for about 6% for the Set 1 while overestimating for about 2% for the Set 2. For Sb, the model describes all the fractions well (RSD < 0.1 for all the points). The situation is the same for Set 2: except one, the most deviating fraction with the RSD of 0.13.

Interelement correlations of Sb are quite the same as for Zn (Table S3, the Supplementary information), with one

relevant exception, Sb leaching is inversely correlated with Si leaching (–0.4). However, with very small changes in Si leaching, this is probably due to a high error in assessment of low leaching values. Without three coarsest fractions, the coefficient of interelement correlation between Sb and Si becomes fairly positive, 0.54, which means that Sb compounds are poorly soluble and accumulated in the particle core along with SiO_2-based minerals [25].

Manganese

For Mn, the coefficients of model correlation are 0.81–0.82 (Table 2). The RSD sums are 4.8–6.6, thus underestimating the entire-range leaching for ca. 36–37%. A fine-fraction range (up to 355 µm) is described well, but for coarser fractions, accurately estimated fractions are alternating with significantly deviating, whereas in the range of 1–22 mm RSD are 0.16–1.24. The two most deviating fractions are 2.0–2.8 mm and 5.6–8.0 mm, with the RSD of 0.72 and 0.83, respectively (Figure S2, Supplementary Information).

Despite large deviations of the model, manganese shows very high coefficients of interelement correlation with all the elements (Table S3, the Supplementary information), showing the highest correlation with nickel, probably due to accumulation of both metals in iron-based phases (the coefficients of correlation of total contents of Mn and Fe, according to the data of [25] is ca. 0.8).

Nickel

The coefficient of correlation for the Set 1 is 0.39, and for the Set 2 is 0.58 (Table 2) and the S-shape is not observed (Fig. 8). The RSD sums are 9.0–9.7, thus underestimating the entire-range leaching for about 71% for the Set 1 and 66% for the Set 2. For Ni, nearly none of the fractions is described accurately by the model. The range of large fractions (2–22.4 mm) deviates the most, with RSD in the range of 0.70–0.98 for the Set 1 and 0.62–0.98 for the Set 2.

Interelement correlations of Ni with all other elements are at the same level of coefficients of 0.4–0.5, and the coefficient of correlation with Si is also non-zero (Table S3, the Supplementary information). As for antimony, the coefficient of interelement correlation Ni–S for all except the three coarsest fractions becomes ca. 0.7, showing that Ni is leached from the particle core, however this cannot be the only reason for the most unpredictable behavior of Ni among the test elments. The most probable reason is than nickel can present in BA in metallic forms [25, 38] and its amounts in MSWI BA are most diverse compared to other metal and common non-metal elements [4, 25, 35, 38, 44, 45, 58–60].

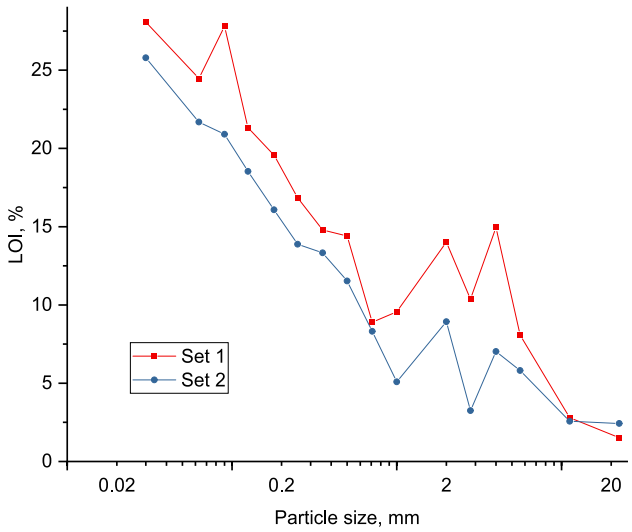

Fig. 10 LOI of the data used in modeling

Discussion

Specific leaching patterns (S-shaped curves with the maximum for the finest fraction and the minimum for the largest for most elements and anions and total leaching, Figs 3, 4, 5, 6, 7, 8 and 10) throughout the particle size range were observed previously [25]. It was shown that the leaching curves throughout the fraction range for many elements are similar in shape, yet no correlation was observed with either particle size or specific surface area [25, 61, 62]. Additionally, it was observed that slow milling led to an increase in leaching due to the possible breakup of the quench layer from the larger grains and its dissolution [4, 22, 25]; thus, it can be assumed that surface area alone is not a suitable predictor for leachability.

Therefore, the study objective was to develop a simple semi-empirical model for estimating the leaching of MSWI BA based on the estimations of both the particle core and quench layer for different size fractions. The primary assumption of the model is that a MSWI BA grain consists of a core and a quench layer of a certain thickness (see the Supplementary information). Thus, the leachabilities of the quench layer and the core are based on the smallest and largest MSWI BA fractions assessed with the one-batch leaching test, and then the amount of quench layer and leachability were calculated for each fraction. The model calculates the ratio between the volume of the quench layer and the entire volume of the particle for each MSWI BA size fraction assuming a uniform thickness of the layer. Additionally, it takes into account a background leaching provided by the

core as proven by the comparison of untreated and treated MSWI BA [4, 25]. The finest fraction is mostly composed of the quench layer [4], so its leaching value is assumed to be representative for the leaching of the quench layer in other fractions and used for calculating the amount of PTEs leaching from the quench layer. The largest fraction contains a small percentage of the quench layer. Thus, the leaching data from the largest fraction is used as a reference (or background) level of MSWI BA leaching that is not or only very slightly affected by the quench layer [4, 31]. Thus, the model considers the leaching value for each fraction corresponding to the volume shares of the quench layer and the core in the particle.

The model is based on two extended sets of the leaching data of 18 particle size fractions of MSWI BA for the particle size range 0–22.4 mm: one for building the model and another for validating it. Unlike previously developed numerical models [52, 53], this approach is based on the leaching data for the most contaminated fine fraction (< 63 µm) and the least contaminated large fraction (> 22.4 mm) of MSWI BA, which is then applied to the entire particle-size range of 18 fractions. To establish the correlation between the elements used for the model building, the total inter-element coefficients of correlation were made for the test elements as well as with silicon leaching (Fig. S4, Supplementary information and total sulfur leaching (Table S3, Supplementary information). It can be seen that all the elements do not correlate well with silicon that is the main element (along with iron and aluminum) of the core of most MSWI BA particles [25] and is not mainly connected with the quench layer [4, 31].

Table 2 shows the overall coefficients of correlation and the total relative residual sums of errors. Based on this data and the interelement coefficients of correlation (Table S3, Supplementary information), all the considered elements in MSWI BA can be separated into three groups. The first group shows a good fit, low total errors (10–20%) and high interelement correlations (coefficients above 0.90). It is comprised of anions (chloride and sulfate), alkali metals (Na^+ and K^+), and alkaline-earth elements (Mg^{2+}, Ca^{2+}, and Sr^{2+}) as well as Cu^{2+}.

The first, largest group (two anions and six cations) is comprised of chloride salts accumulated in the quench layer [6, 39, 42] and the components of CSH [33, 40, 41, 42]. It seems relevant that the model showed a good prediction for copper, which is known as a rather hardly predictable metal in MSWI BA [59, 63] and is a common challenge in BA processing due to high leaching [59, 63]. As previously found, Cu may transform into stable inorganic compounds [64], like hydroxides-sulfates ($Cu_4(OH)_6SO_4 \cdot 1.3H_2O$ etc.) and form readily soluble stable complexes with organic substances [65]. However, the S-shape of the curve for Cu may show that it is mainly present as hydrated oxides and especially chlorides that we previously found to form the large material fraction of the whole BA but can be formed by cooldown or quenching conditions [57]. Considering the complex nature of MSWI BA, multiple factors, which play a role in the leaching of a specific element, and simplification of BA particles in the model, the overall error level attained for the well-fit elements of the first group appears to be satisfactory.

The second group unites elements with a good fit but more significant total error (*ca.* 30%), Ba^{2+}, Zn^{2+}, and Sb^{2+}. Also, these elements have lower interelement coefficients of correlation (Table S3, Supplementary information), ca. 0.7–0.8, between each other and with the elements of the first group. The model predictions for Ba and Sb (Fig. 6) show that the leaching for the most contaminated fraction and the largest fraction do not differ significantly. Unlike the above-described elements of the first group, where the difference between the most and the slightest contaminated fractions would be in the range of an order of magnitude, for Sb, it is about two times, and for Ba, it is approximately the same. One of the possible explanations for this phenomenon would be the size of those cations, their nature as hard acids according to Pearson's principle of hard and soft acids and bases (HSAB), and their tendency to form poorly soluble compounds [66]. Therefore, they might form their phases and/or precipitate on the quench layer but not be adsorbed by it during quenching. This way, through precipitation, they appear in all fractions [17, 67]. However, the behavior of these elements justifies including the leaching of the largest, the least contaminated fraction in the model calculation, to account not for adsorbed compounds only but also for precipitated species that result in a change in shapes of these model curves [15, 17, 68].

For Ba and Sb, which form less soluble compounds but could be accumulated in the quench layer due to the affinity of basic oxides of alkaline-earth metals or sulfate, the model shows fairly satisfactory results with a total error of *ca.* 30%. However, although the general S-shaped curves are visible, the accuracy of the model is reduced due to high leachability of Ba and Sb of the coarse fractions. For Sb, this is confirmed by the precious findings [15, 17, 25, 68]; for Ba, it was previously discussed for the same source of MSWI BA [25]. Probably, the leaching from the fine fractions goes from the quench layer but from very fine particulate matter removed from the quench layer [69]. This is confirmed by the coefficient of interelement correlation between Sb and Ba for all except the coarsest fractions, which is high as 0.74. In our opinion, the behavior of Sb and especially Ba seems to be the drawback of the present model, and it requires some extra work involving other sources of BA. Still, in our opinion, the possibility to use the proposed simple model for elements accumulated in the particle core to account for the leaching from the quench layer seems rather expedient.

Zinc shows much higher values for fine fractions. The reason for that is that metallic zinc is present in MSWI BA, which is different from many other elements [70]. It is highly volatile compared to many other elements and evaporates during incineration, typically emerging in high quantities in fly ash [69]. However, a part of the evaporated zinc may be absorbed by the surface of BA particles, especially the finest fraction with the highest surface area. Still. Even though zinc is considered a difficulty predicted element in MSWI [13, 57, 67], its behavior is described by the model satisfactorily. Also, for Zn, the positive deviation (overestimation) of the model may result from the very diverse distribution of zinc in MSWI BA [57]. Apart from metallic zinc [70], it could be present in soluble compounds like chlorides but may also be present as silicates and phosphates. On one hand, it may be the reason of very low leaching of Zn in coarse fractions [4, 25], however it may be the source of very unpredictable behavior of zinc in fine fractions (Fig. 7), for which many other elements, good fits were found. The coefficients of interelement correlations for Zn with all other elements are average, and they do not change if taking fine or coarse fractions like for other fairly or poorly fit elements. Thus, the investigation of Zn requires some further studies, however, as for the above elements, the workability of the model for this element can be considered a good result at the proof-of-concept stage of model development.

Finally, the rest of the test elements, the third group of Mn^{2+} and Ni^{2+}, shows lower coefficients of correlation of the model and/or significant total errors (> 50%). However, Mn shows very good interelement correlations with the first group, while Ni shows poor correlation with all other elements. Manganese and especially nickel do not follow the S-shape leaching curve, which correlates with previous findings [24]. The reason for the insufficient fit of the model for Mn and Ni might lie in the fact that they tend to form insoluble compounds with iron and accumulated in the same fraction [71]. The increase in the leaching amounts of both metals in fractions over 2 mm may be the result of their accumulation in iron-oxide-rich phases, as shown previously [8, 71]. Combined with the heterogeneity of MSWI BA, and presence of these elements at least partially in metallic form [8, 25, 38] results in the decrease of the model accuracy for those elements (Table 2).

Apart from considering the whole, averaged deviations from the model by total RSD sums, it is expedient to consider fractions that show the maximum deviations. As can be seen for nearly all plots of the elements of the first group, both anions and cations, the model describes well the range of fine fractions and the large one, but for different elements, the artifacts in the ranges 0.3–0.7 mm and above 2 mm remain the same. Also, for nearly all elements, it can be observed that the model does not describe the fraction 4.0–5.6 mm very well, for some elements, the fraction 5.6–8.0 mm is also affected. One of the possible explanations for the first increase for submillimeter-size particles in leaching would be sieving, if contaminated tiny particles adhere to larger particles due to electrostatic effects [33]. This adherence could result in the over-contamination of those fractions and their non-fitting to the proposed model. Figure 5 provides another example of the phenomenon mentioned above for Mg, Ca, and Sr.

The increase in leaching for larger particles might be due to relatively lower amounts of quench-layer-to-core particles in these fractions compared to the overall MSWI BA. It was visibly different after sieving that these fractions contain much more foil, threads, etc., which therefore results in outliers for some elements (Sr, Sb, and Cu). A noticeable number of deviations is also observed for smaller fractions of 0.71–1.0 and 1.0–1.4 mm. This is confirmed by the loss-on-ignition (LOI) data for both sets of MSWI BA (Fig. 10). As can be seen, with an increase in the particle size, LOI decreases. However, the fractions 0.71–8 mm have an increased LOI compared to this trend. This is especially noticeable in the range of 2.0–5.6 mm (Fig. 10). This increase might result from the relatively high amount of unburnt organic matter (leaves, treads, fabrics, etc.) in these large MSWI BA fractions [25]. It is likely that they get enriched in these fractions due to their similar size after incineration. These materials might impact the total leaching because they could disrupt the packing of MSWI particles due to being shaped very differently from the proposed model shape but the regular shape of the MSWI BA particles. The comparison of the total leaching (Fig. 9) with LOI data also shows that the range 2.0–5.6 mm has the maximum deviation from the correlation of these two parameters.

Thus, the modelled values for the entire particle-size range correlate well with the empirically obtained leaching data for total leaching and for elements and anions (Na, K, SO_4^{2-}, Cl^-, Ca, Mg, Sr, Cu, total S and partially Zn) with good or moderate accuracy. Hence, the model predicts the leaching of certain elements well when it is clearly influenced by the composition of the quench layer [4, 6, 31, 37], while the leaching of other elements is influenced by other factors such as presence of metallic forms of elements throughout fractions [8, 25, 33, 38, 70, 71]. It demonstrates that despite the MSWI BA complexity, a simple model can predict the leaching behavior of many elements using a limited set of experimental data: even though the model simplifies the real MSWI BA particles to a great extent [15, 19, 24, 25], it can be used to predict the leaching profile of certain elements using only the leaching values of two fractions as input. Thus, this approach provides the rapid screening of MSWI BA regarding its contamination and an easy assessment of the effectiveness of treatment procedures such as washing or grinding that effect/remove the quench layer [68, 72].

As a whole, the model demonstrates good results for elements of various nature and various roles in MSWI BA, supporting the idea that the quench layer with readily soluble salts and easily released particles has significant influence on the total MSWI BA leaching. The model predicts the leaching behavior of the entire particle size range with an error of 10–20% for ions associated with the soluble salts accumulated in the quench layer. The advantage of this model in comparison with previously proposed [5, 9, 12, 15, 24, 44–48] is its simplicity, independence of chemical equilibria that may change from plant to plant due to a change in the BA composition. Thus, this approach can be used either as a rapid screening of the leaching behavior of an entire MSWI BA batch (to find if it is differently processed, incinerated, or washed) or the estimation of the effectiveness of treatments applied to BA fractions to reduce the leaching that change the BA composition [10, 24, 26, 27, 30, 33, 39, 63, 69].

As proof of concept, the model shows its workability, but this approach has drawbacks and limitations. The main limitation goes from its simplicity and the round-shape character for BA particles and the equal size and composition of the quench layer for all the samples. Probably, this layer is variable, which resulted in some underestimation of the leaching for medium fractions. Also, the model assumes that all the BA particles are the same, but the existing data show that some of the particles may have non-mineral origin as metal or organomineral particles that certainly result in underestimation (seen in millimeter size particles). This second drawback may be partially answered by increasing the number of data sets used for model building and training. It would also be interesting to compare data from different incinerators in different countries to see if the model is applicable in these cases, as in this study, only a Netherlands incineration plant is used. Also, the existing methodology of BA structure and composition as well as leaching properties is well developed but the multicomponent character of BA with possible appearance of new phases may need some more advanced methodological studies involving new methods like X-ray spectroscopy [57, 73, 74] and methodologies developed for other type of waste or natural compounds [74–77]. It may result in more accurate data, especially for the elements with low leaching but still essential or PTE [25, 29, 78].

Conclusions

Thus, as a result of this study, an approach for modelling multielement leaching is proposed that takes into account the quench product layer that is formed during regular post-incineration water-based cooldown process (quenching) of MSWI BA. This approach seems to be a promising and easy way to rapidly estimate the leaching of MSWI BA, but, more importantly, it may predict the leaching of size fractions, which facilitates applying whole or fractionated MSWI BA in various branches of industry that require certain size range of this material. In turn, this can aid selecting fractions that need further treatment, such as washing or grinding, to remove this quench layer. Also, the simplicity of the proposed model towards this aim in comparison with other more complex approaches allows for its potential use in predicting the whole leaching properties of this material.

From viewpoint of another aim, this study, along with previous findings [4, 6, 31, 37] evidences that the MSWI BA water-quenching procedure might have adverse effects on the quality of BA by creating a layer of the quench product. This is especially important for leaching of BA fine fractions due to formation of a large fraction of the quench layer with new highly soluble mineral phases. Therefore, further treatments aimed at improving the quality of the quenched MSWI BA should be directed to undoing the damage caused by the quenching procedure. It appears to be vital to prove the full responsibility of the quench layer for the leaching of the elements that are crucial for the further use in secondary building materials [2–5, 9, 12, 13, 44, 79], such as chloride (which is the main problem often requiring a washing treatment) [39], but also PTEs [23, 36, 60, 67], as to whether the MSWI BA be landfilled or reused [1, 3, 18, 58], it has to match the environmental legislation limits [29, 78]. It can be carefully suggested for consideration that should water quenching be substituted with air (dry) cooling process [79, 80], the level of contamination of BA could drop drastically, especially, for chloride, although the activated status of wet and dry quenching and weathering should also be considered in full. Thus, the material will require less measures to pass the environmental legislation [29, 78]. The proposed modelling approach serves as additional proof of the adverse effect of the water-based quench layer on the leaching. It partially fills the gap in understanding the role of the quench layer by showing similar behavior for elements of various nature including PTEs and with different content levels in MSWI BA.

The proposed model approach is limited due to its simplicity and the condition of the same properties (both the size and the composition) of the quench level for all the size fractions. Also, it does not take into account the existence of non-quenched particles (threads, metal particles, etc.) that may be in a certain size fraction, which manifested in the positive deviation of element composition in submillimeter to millimeter fractions. However, the overall error

of the model makes it suitable for the primary estimation or screening of a BA sample. This study was aimed as proof of concept and cannot show its full potential right now. To further test and improve the model, the high variability of MSWI BA should be taken into account, and more data sets from different batches, different, incineration plants, other countries, etc. should be incorporated to realize the full statistical picture of the model.

Nowadays, a large share of reduce/reuse/recycle-based BA treatment is targeted to undo the damage (mostly related to contamination) from the way of handling the material at nearly all previous steps (waste collection, waste separation, incineration, mixing BA fines with the coarse fraction, and water quenching). Therefore, an attractive route of the research would be to study how handling procedures at all steps contributes to the final properties of the BA product. This may require going a few steps back to begin with the waste and simulate various processes on a laboratory scale, but the outcome might be the generation of several streams of valuable recyclable materials, and either improved qualities of BA and/or a major decrease in the amount of the residuals. In this connection, the proposed approach built or improved by the broader data may be of use both at the stages of basic and applied research.

Supplementary Information The online version contains supplementary material available at https://doi.org/10.1007/s12649-024-02835-3.

Acknowledgements The authors express their gratitude to Mineralz, ENCI, Attero, v.d. Bosch Beton, Struyk Verwo, and CRH Europe Sustainable Concrete Centre for their provision of material, knowledge, and financial support in this project, as well as to the Cement-Concrete-Immobilisates sponsor group at TU Eindhoven: Rijkswaterstaat Grote Projecten en Onderhoud, Graniet-Import Benelux, Kijlstra Betonmortel, Rijkswaterstaat Zee en Delta—District Noord, BTE, Selor, GMB, Geochem Research, Icopal, BN International, Eltomation, Knauf Gips, Hess AAC Systems, Kronos, Joma, Cement&BetonCentrum, Heros, Inashco.

Author contributions Ekaterina Loginova: Conceptualization, Methodology, Investigation, Writing—Original Draft, Visualization; Mikhail Proskurnin: Conceptualization, Methodology, Writing—Review & Editing, Supervision; Katrin Schollbach: Writing—Review & Editing, Supervision; H.J.H. Brouwers: Conceptualization, Writing—Review & Editing, Supervision, Project administration, Resources, Funding acquisition.

Funding NWO/TTW-foundation (project 13318, Development of eco-concretes by using industrial by-products).

Data Availability The datasets generated during and/or analysed during the current study are not publicly available due to restrictions of their use outside of the funding project but are available from the corresponding author on reasonable request.

Declarations

Conflict of interest The authors have no competing interests to declare that are relevant to the content of this article.

References

1. Wiles, C.C.: Municipal solid waste combustion ash: state-of-the-knowledge. J. Hazard. Mater. **47**(1–3), 325–344 (1996). https://doi.org/10.1016/0304-3894(95)00120-4
2. Feng, D., Yu, Y., Wang, J., Liang, S.: Experimental study on municipal solid waste incineration bottom ash as a component of alkali-activated coal gangue–based geopolymer. Environ. Sci. Pollut. Res. **31**(17), 26153–26169 (2024). https://doi.org/10.1007/s11356-024-32945-3
3. Shen, P., Zheng, H., Xuan, D., Lu, J.-X., Poon, C.S.: Feasible use of municipal solid waste incineration bottom ash in ultra-high performance concrete. Cem. Concr. Compos. **114**, 103814 (2020). https://doi.org/10.1016/j.cemconcomp.2020.103814
4. Loginova, E., Schollbach, K., Proskurnin, M., Brouwers, H.J.H.: Municipal solid waste incineration bottom ash fines: transformation into a minor additional constituent for cements. Resour. Conserv. Recycl. **166**, 105354 (2021). https://doi.org/10.1016/j.resconrec.2020.105354
5. Engelsen, C.J., van der Sloot, H.A., Petkovic, G.: Long-term leaching from recycled concrete aggregates applied as sub-base material in road construction. Sci. Total. Environ. **587–588**, 94–101 (2017). https://doi.org/10.1016/j.scitotenv.2017.02.052
6. Alam, Q., Lazaro, A., Schollbach, K., Brouwers, H.J.H.: Chemical speciation, distribution and leaching behavior of chlorides from municipal solid waste incineration bottom ash. Chemosphere **241**, 124985 (2020). https://doi.org/10.1016/j.chemosphere.2019.124985
7. Bayuseno, A.P., Schmahl, W.W.: Understanding the chemical and mineralogical properties of the inorganic portion of MSWI bottom ash. Waste Manag. **30**(8–9), 1509–1520 (2010). https://doi.org/10.1016/j.wasman.2010.03.010
8. Del Valle-Zermeno, R., Gomez-Manrique, J., Giro-Paloma, J., Formosa, J., Chimenos, J.M.: Material characterization of the MSWI bottom ash as a function of particle size. Effects of glass recycling over time. Sci. Total Environ. **581–582**, 897–905 (2017). https://doi.org/10.1016/j.scitotenv.2017.01.047
9. Lynn, C.J., Ghataora, G.S., Dhir Obe, R.K.: Municipal incinerated bottom ash (MIBA) characteristics and potential for use in road pavements. Int. J. Pavement Res. and Technol. **10**(2), 185–201 (2017). https://doi.org/10.1016/j.ijprt.2016.12.003
10. Holm, O., Simon, F.G.: Innovative treatment trains of bottom ash (BA) from municipal solid waste incineration (MSWI) in Germany. Waste Manag. **59**, 229–236 (2017). https://doi.org/10.1016/j.wasman.2016.09.004
11. Meawad, A.S., Bojinova, D.Y., Pelovski, Y.G.: An overview of metals recovery from thermal power plant solid wastes. Waste Manag. **30**(12), 2548–2559 (2010). https://doi.org/10.1016/j.wasman.2010.07.010
12. van der Sloot, H.A., Kosson, D.S., van Zomeren, A.: Leaching, geochemical modelling and field verification of a municipal solid waste and a predominantly non-degradable waste landfill. Waste Manag. **63**, 74–95 (2017). https://doi.org/10.1016/j.wasman.2016.07.032
13. Funari, V., Braga, R., Bokhari, S.N., Dinelli, E., Meisel, T.: Solid residues from Italian municipal solid waste incinerators: a source for "critical" raw materials. Waste Manag. **45**, 206–216 (2015). https://doi.org/10.1016/j.wasman.2014.11.005
14. Meima, J.A., Comans, R.N.J.: Overview of Geochemical Processes Controlling Leaching Characteristics of MSWI Bottom Ash. In: Goumans JJJM, Senden GJ, van der Sloot HA, editors. Waste Materials in Construction - Putting Theory into Practice, Proceedings of the International Conference on the Environment and Technical Implications of Construction with Alternative

Materials. Studies in Environmental Science.Elsevier: (1997). p. 447-457.
15. Dijkstra, J.J., van der Sloot, H.A., Comans, R.N.J.: The leaching of major and trace elements from MSWI bottom ash as a function of pH and time. Appl. Geochem. **21**(2), 335–351 (2006). https://doi.org/10.1016/j.apgeochem.2005.11.003
16. Van Zomeren, A., Comans, R.N.: Contribution of natural organic matter to copper leaching from municipal solid waste incinerator bottom ash. Environ. Sci. Technol. **38**(14), 3927–3932 (2004). https://doi.org/10.1021/es035266v
17. Verbinnen, B., Van Caneghem, J., Billen, P., Vandecasteele, C.: Long term leaching behavior of antimony from MSWI bottom ash: influence of mineral additives and of organic acids. Waste and Biomass Valorization **8**(7), 2545–2552 (2016). https://doi.org/10.1007/s12649-016-9796-6
18. Piltz, G., Annema, J.A., Pesch, U.: Experts' perspectives on the sustainability and risks of freely applicable MSWI bottom ash: a Q-methodology study in the Netherlands. Environ. Dev. Sustain. **26**(10), 25785–25809 (2023). https://doi.org/10.1007/s10668-023-03707-x
19. Caprai, V., Florea, M.V.A., Brouwers, H.J.H.: Evaluation of the influence of mechanical activation on physical and chemical properties of municipal solid waste incineration sludge. J. Environ. Manage. **216**, 133–144 (2018). https://doi.org/10.1016/j.jenvman.2017.05.024
20. Rivard-Lentz, D., Sweeney, L., Demars, K.: Incinerator Bottom Ash as a Soil Substitute: Physical and Chemical Behavior, in: Testing Soil Mixed with Waste or Recycled Materials. In: Wasemiller MA, Hoddinott KB, editors. STP1275-EB. Testing Soil Mixed with Waste or Recycled Materials. PO Box C700, West Conshohocken, PA 19428–2959,: ASTM International; 1997. p. 246–262.
21. Speiser, C., Baumann, T., Niessner, R.: Morphological and chemical characterization of calcium-hydrate phases formed in alteration processes of deposited municipal solid waste incinerator bottom ash. Environ. Sci. Technol. **34**(23), 5030–5037 (2000). https://doi.org/10.1021/es990739c
22. Loginova, E., Schollbach, K., Proskurnin, M., Brouwers, H.J.H.: Mechanical performance and microstructural properties of cement mortars containing MSWI BA as a minor additional constituent. Case Studies in Constr. Mater. **18**, e01701 (2023). https://doi.org/10.1016/j.cscm.2022.e01701
23. De Matteis, C., Mantovani, L., Tribaudino, M., Bernasconi, A., Destefanis, E., Caviglia, C., et al.: Sequential extraction procedure of municipal solid waste incineration (MSWI) bottom ash targeting grain size and the amorphous fraction. Front. Environ. Sci. (2023). https://doi.org/10.3389/fenvs.2023.1254205
24. Kitamura, H., Sawada, T., Shimaoka, T., Takahashi, F.: Geochemically structural characteristics of municipal solid waste incineration fly ash particles and mineralogical surface conversions by chelate treatment. Environ. Sci. Pollut. Res. Int. **23**(1), 734–743 (2016). https://doi.org/10.1007/s11356-015-5229-5
25. Loginova, E., Volkov, D.S., van de Wouw, P.M.F., Florea, M.V.A., Brouwers, H.J.H.: Detailed characterization of particle size fractions of municipal solid waste incineration bottom ash. J. Clean. Prod. **207**, 866–874 (2019). https://doi.org/10.1016/j.jclepro.2018.10.022
26. Arickx, S., Van Gerven, T., Knaepkens, T., Hindrix, K., Evens, R., Vandecasteele, C.: Influence of treatment techniques on Cu leaching and different organic fractions in MSWI bottom ash leachate. Waste Manag. **27**(10), 1422–1427 (2007). https://doi.org/10.1016/j.wasman.2007.03.015
27. Arickx, S., Van Gerven, T., Vandecasteele, C.: Accelerated carbonation for treatment of MSWI bottom ash. J. Hazard. Mater. **137**(1), 235–243 (2006). https://doi.org/10.1016/j.jhazmat.2006.01.059
28. Bertolini, L., Carsana, M., Cassago, D., Quadrio Curzio, A., Collepardi, M.: MSWI ashes as mineral additions in concrete. Cem. Concr. Res. **34**(10), 1899–1906 (2004). https://doi.org/10.1016/j.cemconres.2004.02.001
29. Keulen, A., van Zomeren, A., Harpe, P., Aarnink, W., Simons, H.A.E., Brouwers, H.J.H.: High performance of treated and washed MSWI bottom ash granulates as natural aggregate replacement within earth-moist concrete. Waste Manag. **49**, 83–95 (2016). https://doi.org/10.1016/j.wasman.2016.01.010
30. Saikia, N., Mertens, G., Van Balen, K., Elsen, J., Van Gerven, T., Vandecasteele, C.: Pre-treatment of municipal solid waste incineration (MSWI) bottom ash for utilisation in cement mortar. Constr. Build. Mater. **96**, 76–85 (2015). https://doi.org/10.1016/j.conbuildmat.2015.07.185
31. Inkaew, K., Saffarzadeh, A., Shimaoka, T.: Modeling the formation of the quench product in municipal solid waste incineration (MSWI) bottom ash. Waste Manag. **52**, 159–168 (2016). https://doi.org/10.1016/j.wasman.2016.03.019
32. Vateva, I., Laner, D.: Grain-size specific characterisation and resource potentials of municipal solid waste incineration (MSWI) bottom ash: a German case study. Resources **9**(6), 66 (2020). https://doi.org/10.3390/resources9060066
33. Alam, Q., Florea, M.V.A., Schollbach, K., Brouwers, H.J.H.: A two-stage treatment for Municipal Solid Waste Incineration (MSWI) bottom ash to remove agglomerated fine particles and leachable contaminants. Waste Manag. **67**, 181–192 (2017). https://doi.org/10.1016/j.wasman.2017.05.029
34. Wunsch, P., Greilinger, C., Bieniek, D., Kettrup, A.: Investigation of the binding of heavy metals in thermally treated residues from waste incineration. Chemosphere **32**(11), 2211–2218 (1996). https://doi.org/10.1016/0045-6535(96)00123-3
35. Zhu, Y., Zhao, Y., Zhao, C., Gupta, R.: Physicochemical characterization and heavy metals leaching potential of municipal solid waste incinerated bottom ash (MSWI-BA) when utilized in road construction. Environ. Sci. Pollut. Res. **27**(12), 14184–14197 (2020). https://doi.org/10.1007/s11356-020-08007-9
36. Li, Y.-M., Wu, X.-Q., Wang, L.-J., Li, R.-Q., Huang, T.-Y., Wen, X.-Q.: Comparative study on utilization of different types of municipal solid waste incineration bottom ash for clinker sintering. J. Mater. Cycles Waste Manage. **22**(6), 1828–1843 (2020). https://doi.org/10.1007/s10163-020-01067-6
37. Marchese, F., Genon, G.: Effect of leaching behaviour by quenching of bottom ash from MSW incineration. Waste Manag Res **29**(10 Suppl), 39–47 (2011). https://doi.org/10.1177/0734242X10387848
38. Huber, F., Blasenbauer, D., Aschenbrenner, P., Fellner, J.: Chemical composition and leachability of differently sized material fractions of municipal solid waste incineration bottom ash. Waste Manag. **95**, 593–603 (2019). https://doi.org/10.1016/j.wasman.2019.06.047
39. Yang, S., Saffarzadeh, A., Shimaoka, T., Kawano, T.: Existence of Cl in municipal solid waste incineration bottom ash and dechlorination effect of thermal treatment. J. Hazard. Mater. **267**, 214–220 (2014). https://doi.org/10.1016/j.jhazmat.2013.12.045
40. Saffarzadeh, A., Shimaoka, T., Wei, Y., Gardner, K.H., Musselman, C.N.: Impacts of natural weathering on the transformation/neoformation processes in landfilled MSWI bottom ash: a geoenvironmental perspective. Waste Manag. **31**(12), 2440–2454 (2011). https://doi.org/10.1016/j.wasman.2011.07.017
41. Zhou, Y., Zheng, H., Qiu, Y., Zou, X., Huang, J.: A molecular dynamics study on the structure, interfaces, mechanical properties, and mechanisms of a calcium silicate hydrate/2D-silica

nanocomposite. Front. Mater. (2020). https://doi.org/10.3389/fmats.2020.00127
42. Ito, R., Dodbiba, G., Fujita, T., Ahn, J.W.: Removal of insoluble chloride from bottom ash for recycling. Waste Manag. **28**(8), 1317–1323 (2008). https://doi.org/10.1016/j.wasman.2007.05.015
43. Arickx, S., Van Gerven, T., Boydens, E., L'hoest, P., Blanpain, B., Vandecasteele, C.: Speciation of Cu in MSWI bottom ash and its relation to Cu leaching. Appl. Geochem. **23**(12), 3642–3650 (2008). https://doi.org/10.1016/j.apgeochem.2008.09.006
44. Chimenos, J.M., Segarra, M., Fernández, M.A., Espiell, F.: Characterization of the bottom ash in municipal solid waste incinerator. J. Hazard. Mater. **64**(3), 211–222 (1999). https://doi.org/10.1016/s0304-3894(98)00246-5
45. Forteza, R., Far, M., Segui, C., Cerda, V.: Characterization of bottom ash in municipal solid waste incinerators for its use in road base. Waste Manag. **24**(9), 899–909 (2004). https://doi.org/10.1016/j.wasman.2004.07.004
46. Müller, U., Rübner, K.: The microstructure of concrete made with municipal waste incinerator bottom ash as an aggregate component. Cem. Concr. Res. **36**(8), 1434–1443 (2006). https://doi.org/10.1016/j.cemconres.2006.03.023
47. Déchaux, C., Nitschelm, L., Giard, L., Bioteau, T., Sessiecq, P., Aissani, L.: Development of the regionalised municipal solid waste incineration (RMWI) model and its application to France. Int. J. Life Cycle Assess. **22**(10), 1514–1542 (2017). https://doi.org/10.1007/s11367-017-1268-0
48. Koehler, A., Peyer, F., Salzmann, C., Saner, D.: Probabilistic and technology-specific modeling of emissions from municipal solid-waste incineration. Environ. Sci. Technol. **45**(8), 3487–3495 (2011). https://doi.org/10.1021/es1021763
49. Chimenos, J.M., Fernandez, A.I., Miralles, L., Segarra, M., Espiell, F.: Short-term natural weathering of MSWI bottom ash as a function of particle size. Waste Manag. **23**(10), 887–895 (2003). https://doi.org/10.1016/S0956-053X(03)00074-6
50. Meima, J.A., Comans, R.N.J.: Geochemical modeling of weathering reactions in municipal solid waste incinerator bottom ash. Environ. Sci. Technol. **31**(5), 1269–1276 (1997). https://doi.org/10.1021/es9603158
51. Quina, M.J., Bordado, J.C., Quinta-Ferreira, R.M.: The influence of pH on the leaching behaviour of inorganic components from municipal solid waste APC residues. Waste Manag. **29**(9), 2483–2493 (2009). https://doi.org/10.1016/j.wasman.2009.05.012
52. Park, J.Y., Batchelor, B.: A multi-component numerical leach model coupled with a general chemical speciation code. Water Res. **36**(1), 156–166 (2002). https://doi.org/10.1016/s0043-1354(01)00207-x
53. Dijkstra, J.J., van der Sloot, H.A., Comans, R.N.: Process identification and model development of contaminant transport in MSWI bottom ash. Waste Manag. **22**(5), 531–541 (2002). https://doi.org/10.1016/s0956-053x(01)00034-4
54. Dijkstra, J.J., Meeussen, J.C.L., Van der Sloot, H.A., Comans, R.N.J.: A consistent geochemical modelling approach for the leaching and reactive transport of major and trace elements in MSWI bottom ash. Appl. Geochem. **23**(6), 1544–1562 (2008). https://doi.org/10.1016/j.apgeochem.2007.12.032
55. Dahl, O., Nurmesniemi, H., Pöykiö, R., Watkins, G.: Comparison of the characteristics of bottom ash and fly ash from a medium-size (32 MW) municipal district heating plant incinerating forest residues and peat in a fluidized-bed boiler. Fuel Process. Technol. **90**(7–8), 871–878 (2009). https://doi.org/10.1016/j.fuproc.2009.04.013
56. Templeton, C.C.: Solubility of barium sulfate in sodium chloride solutions from 25° to 95 °C. J. Chem. Eng. Data **5**(4), 514–516 (1960). https://doi.org/10.1021/je60008a028
57. Rissler, J., Klementiev, K., Dahl, J., Steenari, B.-M., Edo, M.: Identification and quantification of chemical forms of Cu and Zn in MSWI ashes using XANES. Energy Fuels **34**(11), 14505–14514 (2020). https://doi.org/10.1021/acs.energyfuels.0c02226
58. Zhang, H., He, P.J., Shao, L.M.: Fate of heavy metals during municipal solid waste incineration in Shanghai. J. Hazard. Mater. **156**(1–3), 365–373 (2008). https://doi.org/10.1016/j.jhazmat.2007.12.025
59. Meima, J.A., van der Weijden, R.D., Eighmy, T.T., Comans, R.N.J.: Carbonation processes in municipal solid waste incinerator bottom ash and their effect on the leaching of copper and molybdenum. Appl. Geochem. **17**(12), 1503–1513 (2002). https://doi.org/10.1016/s0883-2927(02)00015-x
60. Weiksnar, K.D., Marks, E.J., Deaderick, M.J., Meija-Ruiz, I., Ferraro, C.C., Townsend, T.G.: Impacts of advanced metals recovery on municipal solid waste incineration bottom ash: aggregate characteristics and performance in portland limestone cement concrete. Waste Manag. **187**, 70–78 (2024). https://doi.org/10.1016/j.wasman.2024.07.008
61. Dabo, D., Badreddine, R., De Windt, L., Drouadaine, I.: Ten-year chemical evolution of leachate and municipal solid waste incineration bottom ash used in a test road site. J. Hazard. Mater. **172**(2–3), 904–913 (2009). https://doi.org/10.1016/j.jhazmat.2009.07.083
62. Liu, Y., Li, Y., Li, X., Jiang, Y.: Leaching behavior of heavy metals and PAHs from MSWI bottom ash in a long-term static immersing experiment. Waste Manag. **28**(7), 1126–1136 (2008). https://doi.org/10.1016/j.wasman.2007.05.014
63. Yao, J., Li, W.B., Tang, M., Fang, C.R., Feng, H.J., Shen, D.S.: Effect of weathering treatment on the fractionation and leaching behavior of copper in municipal solid waste incinerator bottom ash. Chemosphere **81**(5), 571–576 (2010). https://doi.org/10.1016/j.chemosphere.2010.08.038
64. Meima, J.A., Comans, R.N.J.: The leaching of trace elements from municipal solid waste incinerator bottom ash at different stages of weathering. Appl. Geochem. **14**(2), 159–171 (1999). https://doi.org/10.1016/S0883-2927(98)00047-X
65. Sunda, W.G., Lewis, J.A.M.: Effect of complexation by natural organic ligands on the toxicity of copper to a unicellular alga, Monochrysis lutheri1. Limnol. Oceanogr. **23**(5), 870–876 (2003). https://doi.org/10.4319/lo.1978.23.5.0870
66. Kraml, G., Gritzner, G.: Electrochemical measurements in the solvents hexamethylphosphoric triamide and hexamethylthiophosphoric triamide. J. Chem. Soc., Faraday Trans. Phys. Chem. in Condens. Phases **81**(11), 2875–2888 (1985). https://doi.org/10.1039/f19858102875
67. Alam, Q., Schollbach, K., Rijnders, M., van Hoek, C., van der Laan, S., Brouwers, H.J.H.: The immobilization of potentially toxic elements due to incineration and weathering of bottom ash fines. J. Hazard Mater. **379**, 120798 (2019). https://doi.org/10.1016/j.jhazmat.2019.120798
68. Cornelis, G., Van Gerven, T., Vandecasteele, C.: Antimony leaching from MSWI bottom ash: modelling of the effect of pH and carbonation. Waste Manag. **32**(2), 278–286 (2012). https://doi.org/10.1016/j.wasman.2011.09.018
69. Loginova, E., Proskurnin, M., Brouwers, H.J.H.: Municipal solid waste incineration (MSWI) fly ash composition analysis: a case study of combined chelatant-based washing treatment efficiency. J. Environ. Manage. **235**, 480–488 (2019). https://doi.org/10.1016/j.jenvman.2019.01.096
70. Łukowski, A.: Fractions of zinc, chromium and cobalt in municipal solid waste incineration bottom ash. J. Ecol. Eng. **23**(3), 12–16 (2022). https://doi.org/10.12911/22998993/145765
71. Łukowski, A.: Fractional composition of nickel, manganese and iron in municipal solid waste incineration bottom ash. J. Ecol.

Eng. **23**(11), 235–240 (2022). https://doi.org/10.12911/22998993/154600
72. Todorovic, J., Ecke, H.: Demobilisation of critical contaminants in four typical waste-to-energy ashes by carbonation. Waste Manag. **26**(4), 430–441 (2006). https://doi.org/10.1016/j.wasman.2005.11.011
73. De Matteis, C., Pollastri, S., Mantovani, L., Tribaudino, M.: Potentially toxic elements speciation in bottom ashes from a municipal solid waste incinerator: a combined SEM-EDS, μ-XRF and μ-XANES study. Environ. Adv. **15**, 100453 (2024). https://doi.org/10.1016/j.envadv.2023.100453
74. Gan, M., Xing, J., Tang, Q., Ji, Z., Fan, X., Zheng, H., et al.: Basic research on Co-treatment of municipal solid waste incineration fly ash and municipal sludge for energy-saving melting. ACS Omega **7**(49), 45153–45164 (2022). https://doi.org/10.1021/acsomega.2c05598
75. Kotelnikova, A.D., Rogova, O.B., Karpukhina, E.A., Solopov, A.B., Levin, I.S., Levkina, V.V., et al.: Assessment of the structure, composition, and agrochemical properties of fly ash and ash-and-slug waste from coal-fired power plants for their possible use as soil ameliorants. J. Clean. Prod. **333**, 130088 (2022). https://doi.org/10.1016/j.jclepro.2021.130088
76. Chen, Z., Chang, W., Jiang, X., Lu, S., Buekens, A., Yan, J.: Leaching behavior of circulating fluidised bed MSWI air pollution control residue in washing process. Energies **9**(9), 743 (2016). https://doi.org/10.3390/en9090743
77. Volkov, D.S., Rogova, O.B., Ovseenko, S.T., Odelskii, A., Proskurnin, M.A.: Element composition of fractionated water-extractable soil colloidal particles separated by track-etched membranes. Agrochemicals **2**(4), 561–580 (2023). https://doi.org/10.3390/agrochemicals2040032
78. Aubert, J.E., Husson, B., Sarramone, N.: Utilization of municipal solid waste incineration (MSWI) fly ash in blended cement Part 2. Mechanical strength of mortars and environmental impact. J. Hazard Mater. **146**(1–2), 12–19 (2007). https://doi.org/10.1016/j.jhazmat.2006.11.044
79. Bawab, J., Khatib, J., Kenai, S., Sonebi, M.: A review on cementitious materials including municipal solid waste incineration bottom ash (MSWI-BA) as aggregates. Buildings **11**(5), 179 (2021). https://doi.org/10.3390/buildings11050179
80. Yang, S., Saffarzadeh, A., Shimaoka, T., Kawano, T., Kakuta, Y.: The impact of thermal treatment and cooling methods on municipal solid waste incineration bottom ash with an emphasis on Cl. Environ. Technol. **37**(20), 2564–2571 (2016). https://doi.org/10.1080/09593330.2016.1155651

Authors and Affiliations

E. Loginova[1] · M. A. Proskurnin[2] · K. Schollbach[1] · H. J. H. Brouwers[1]

✉ E. Loginova
kitti.loginova@gmail.com

✉ M. A. Proskurnin
proskurnin@gmail.com

[1] Unit Building Physics and Services, Department of the Built Environment, Eindhoven University of Technology, P.O. Box 513, 5600 MB Eindhoven, The Netherlands

[2] Chemistry Department, Lomonosov Moscow State University, Leninskie Gory 1-3, GSP-1, Moscow, Russia 119991